JOURNAL OF MATERIALS SCIENCE 21 (1986) 1–25

Review
Ion-based methods for optical thin film deposition

P. J. MARTIN
CSIRO Division of Applied Physics, Sydney 2070, Australia

The optical properties of the dielectric oxide films SiO_2, Al_2O_3, TiO_2, ZrO_2, CeO_2 and Ta_2O_5 produced by ion-based techniques have been reviewed. The influence of ion bombardment during deposition is discussed in some detail and the various production techniques are described. Recent results on the deposition and properties of diamond-like carbon films are also reviewed. Finally, some examples of the practical applications of high quality dielectric oxide films are given.

1. Introduction

Vacuum-deposited optical coatings have been available for nearly half a century, but the quest for better and more reproducible films is still continuing in order to meet the exacting needs of modern precision optics. Early coatings were simple anti-reflective, high-reflectance, or beamsplitter coatings comprising only a few layers. Present day applications however, require high performance coatings such as those employed in high power lasers and laser gyroscopes where reflectance and stability are important factors.

The ideal optical multilayer coating consists of homogeneous layers, each layer with bulk properties and the film interfaces parallel and smooth. The spectral characteristics for such a system can be readily calculated. In practice vacuum deposited films vary significantly in many respects from bulk materials. The adhesion to the substrate and neighbouring layers may be poor, the interfaces and surfaces rough, and in some cases the stress in the film sufficiently high to cause mechanical failure. A particularly serious problem in optical film technology arises when the freshly deposited single or multilayer structure is exposed to the atmosphere. It is frequently found that the optical properties vary in an unpredictable and irreversible fashion, depending upon the relative humidity.

Film reproducibility depends to a large extent upon the process parameters. The relationship between film properties and process parameters has been summarized by Ritter [1] and is reproduced in Table I. Two dots represent a strong dependency, one dot an established dependency, and a dot in parenthesis indicates a possible dependence. This table demonstrates the complexity of the interplay between film properties and preparation conditions, particularly when a variation in one parameter may alter several properties. The traditional methods of optical film deposition have largely been thermal evaporation either by resistive heating or by electron- beam evaporation, where the problems indicated in Table I are frequently encountered.

In recent years the introduction of sputter deposition and ion-assisted technology has resulted in very significant improvements in film quality control and optical properties. The key feature of these techniques is the use of the ions (a) to sputter deposit material, (b) in direct deposition of ionized vapour, (c) in adding activation energy or chemical activity to the growing film, or combinations of these effects. A further application of ions is the implantation of very high energy particles to form buried layers in substrate materials. The ions may be used in a plasma region or high vacuum region (ion beam techniques), and the kinetic energies fall within a range of a few eV to a few hundred keV (ion implantation). It is therefore necessary to have some basic understanding of the ion–surface interaction phenomena and their dependence on ion energy and ion mass.

2. Ion–surface interaction processes

The importance of ion–surface interaction processes in optical film deposition depends upon the particular deposition process employed. Ions in general can transfer energy, momentum and charge by varying degrees. In all cases a complex variety of processes simultaneously occur whenever energetic particles interact with a substrate or growing film. For a comprehensive description of these processes, the reader is referred to a number of excellent reviews in the literature [2–5]. In the present discussion the following processes illustrated in Fig. 1 will be considered: sputtering, ion reflection, penetration and trapping. In addition, some chemical effects are discussed.

2.1. Sputtering

One of the principal effects during ion bombardment of a solid surface is the ejection or sputtering of the surface atoms. The energetic primary particles lose energy in a series of elastic and inelastic collisions with target atoms. The recoiling target atoms initiate secondary collisions in a collision cascade. Some energy may eventually be transferred to the surface

0022–2461/86 $03.00 + .12

TABLE I Influence of process parameters on film properties [1]

Film property	Substrate material	Substrate cleaning	Starting material	Glow discharge	Evaporation method	Rate	Pressure	Vapour	Substrate temperature
Refractive index			●	●		●●	●●	●●	●●
Transmission			●	●	●	(●)	(●)		(●)
Scattering	●●	●	(●)	(●)	●	(●)	●●	●	●●
Geometric thickness		●		●		●	●	●	●●
Stress	●●	(●)	●●			●	●	●	●
Adherence	●	●●		●●	●	●	●	●	●
Hardness	●	●		●		●	●●	●	●●
Temperature stability	●					●	●	●	●●
Insolubility	(●)	●	●	●		●	●●	●	●●
Resistance to laser radiation	(●)	●	●	●	●	●			●
Defects	●●	●	●	●	●●	●	(●)		●

atoms which will be ejected if the surface binding energy is overcome. The cascade has a typical radius of 10 nm and sputtering results from collision sequences $\lesssim 5$ atomic layers beneath the surface [6].

The most successful sputtering model to date is that due to Sigmund [7–9]. If we consider the low energy regime (1 keV and below) the sputtering yield, $Y(E)$, is given as:

$$Y(E) = 0.3 \frac{M_i M}{(M_i + M)^2} \alpha\left(\frac{M}{M_i}\right) \frac{E_0}{U_0} \quad (1)$$

where M_i and M are the atomic masses of the incident ion and target atom respectively, $\alpha(M/M_i)$ is a numerically calculated function varying from 0.15 to 1.5, E_0 the energy of the ion, and U_0 is the surface binding energy of the target atom. The model has been tested experimentally [10] and found to be in reasonable agreement for 500 eV argon ions on various targets.

The model is not suitable for threshold sputtering conditions, i.e. $E_0 \leqslant U_0$ and a universal model has been developed by Bohdansky *et al.* [11]. In this model the sputtering yield is given by:

$$Y(E) = 6.4 \times 10^{-3} M \gamma^{5/3} E_0^{1/4} (1 - E^{*-1})^{7/2} \quad (2)$$

where $E^* = E_0/E_{th}$, E_{th} is the threshold energy for sputtering, and $\gamma = 4M_iM/(M_i + M)^2$. This model does predict zero yield for $E = E_{th}$ and is in good agreement with experimental data for very low mass ions and argon bombardment of metals.

The most complete set of experimental sputtering yields available has been compiled by Andersen and Bay [12] covering most ions over the energy range 0.1 to 100 keV. The situation is far less satisfactory for the sputtering of compound targets since there exists no universal sputtering theory and only limited experimental data.

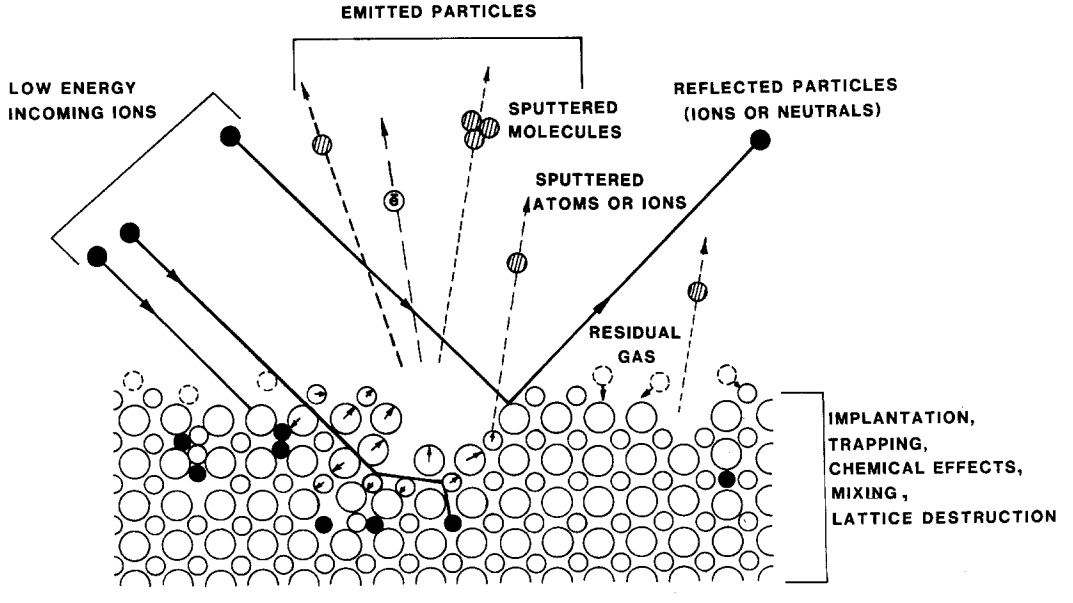

Figure 1 General ion-surface interaction processes.

2.1.1. Preferential sputtering

During the sputtering of compounds the most volatile species is preferentially sputtered, for example oxygen from oxides. A concentration gradient or altered layer is created at the target surface. Under steady state conditions the surface composition of a multi-element target will adjust itself to balance the elemental sputtering yields. The degree of preferential sputtering depends upon projectile energy, mass and target atom binding energy, but can be severe even for low energy e.g. (less than 3 keV) He^+ on Ta_2O_5 [13]. For compounds with large differences in mass, a greater proportion of the bombardment energy is deposited into the sub-lattice containing the lighter element and the effect is predominant at lower primary energies.

However, in the case of film deposition by sputtering from compounds, under steady state the composition of the sputtered flux is the same as the bulk concentration of the target. Compositional changes due to ion bombardment can be significant where growing films are irradiated.

Oxide systems generally become depleted of oxygen under ion bombardment and reduction of oxidized molybdenum, tungsten, niobium, tantalum, titanium, zirconium, silicon and bismuth has been observed [14]. Many measurements of preferential sputtering have been reported and Coburn [15] has compiled data on metal alloys and oxides. Kelly and Lam [16] have reported that the sputtering yields of many oxides are in accordance with Sigmund's theory i.e. Y is proportional to U_0^{-1} where U_0 is the surface binding energy. In addition to compositional variations bombardment-induced structural changes have been observed for many oxide systems. These effects have variously been attributed to thermal-spike effects, displacement spikes and bond-type criteria [17, 18].

2.1.2. Energies of sputtered particles

Film properties are largely determined by the energies of the depositing atoms. In conventional evaporation the maximum energy is only ~ 0.1 eV whereas sputtered particle energy distributions peak at 1 to 2 eV and extend to about 100 eV. Fig. 2 shows that the peak in the energy distribution of sputtered titanium shifts only slightly with the incident particle mass and energy [19]. In general the sputtered atom energy distributions follow an E^{-2} dependence.

A small percentage of the sputtered material is ionized and has a similar energy distribution to the neutral component but peaking at a higher energy of about 5 to 10 eV. The secondary ion yield is sensitive to matrix effects and is greatly enhanced in the presence of oxygen [20].

In sputter deposition at high gas pressure, frequent collisions between sputtered atoms and residual gas decrease the energy of the depositing flux. This process is referred to as thermalization. Meyer *et al.* [21] have calculated the energy distribution of niobium and copper atoms and the effect of argon gas pressure as a function of distance from the target surface. The energy distribution can be adjusted by varying the sputtering conditions, affording greater control over the depositing atom energy than is possible with evaporation. More recent computations using Monte

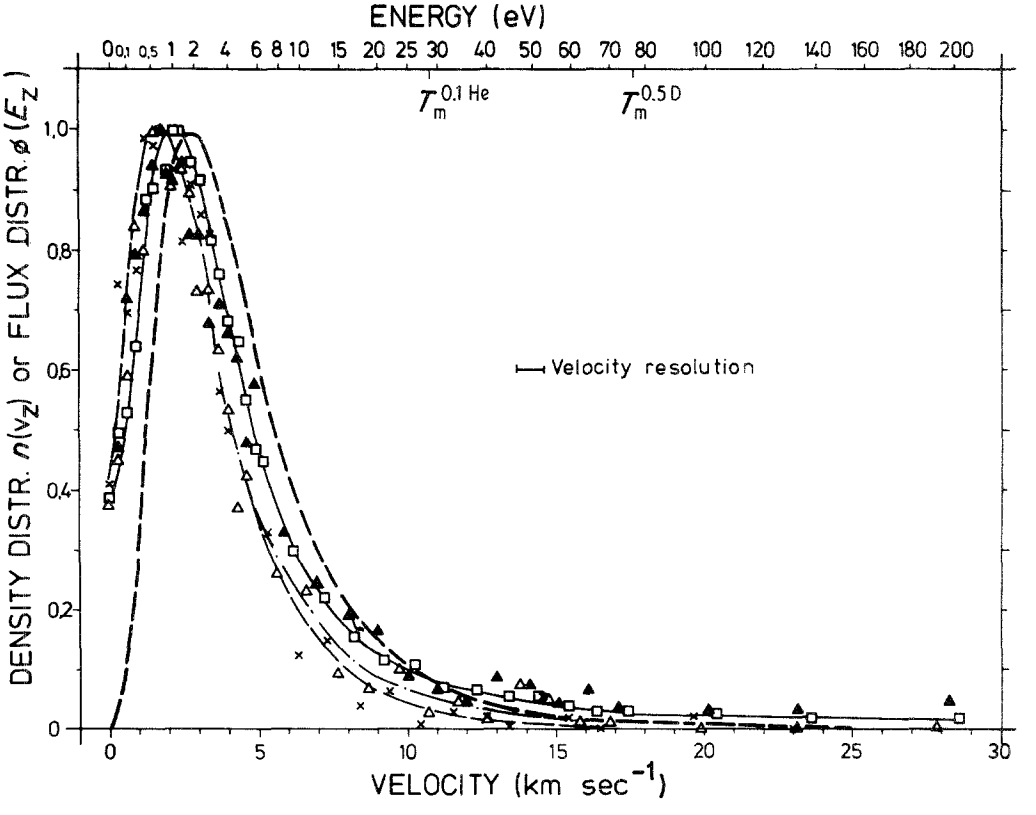

Figure 2 Density distribution $n(v_z)$ of sputtered titanium atoms as a function of energy [19]. — — Theory. Ions, □ 8 keV He^+, × 0.1 keV He^+, ▲ 2.5 keV D^+, △ 0.5 keV D^+. $T_m = 4M_iM/(M_i + M)^2$; resolution of the velocity/energy measurement is given by the error bar.

Carlo simulation show that sputtered particles can be selectively thermalized depending upon the elements present [22, 23].

2.2. Damage due to sputtering

Ion-surface interaction generally leads to displacement of surface and bulk atoms. Each collision cascade on average can displace $N_D(E_1) = E_1/4E_d$ atoms where E_d is in the range 10 to 50 eV [3]. For example, 1 keV argon can displace 12 atoms in nickel and 25 in silicon and sputter 3 nickel atoms and 1 silicon [7]. The collision cascade event is completed within 10^{-13} sec and a large number of the vacancies and interstitials are eliminated. Thermal or displacement spikes may occur and surfaces may undergo crystalline–amorphous transitions [17]. Other effects of importance are surface atoms or primary recoil atoms being pushed into the target or substrate (recoil implantation) and atoms being transported over short distances during the collision cascade (cascade mixing). The creation of surface defects by ion bombardment can enhance diffusion processes and accelerate compound formation such as oxides or nitrides [24].

2.3. Ion reflection

Thin films deposited by ion-beam sputtering of a target may be subjected to significant bombardment by primary particles scattered off the target surface on to the growing film. The growing film will then contain a percentage of primary particles as well as being subjected to radiation-induced structural changes.

At low energies it is possible for light ions to be backscattered from heavier target atoms, for example, He^+, Ne^+ and Ar^+ from copper and silver surfaces. The energy E_1 of the backscattered ion of mass M_1 can be calculated for a given scattering angle θ and target atom mass M_2 from binary collision theory [3],

$$E/E_0 = \left[\frac{\cos\theta \pm (\mu^2 - \sin^2\theta)^{1/2}}{1 + \mu}\right]^2 \quad (3)$$

where $\mu = M_2/M_1$. This approximation for the scattered ion energy assumes that the collisions are elastic. Inelastic processes such as collisional excitation can reduce the observed scattered energies. In addition, low energy ions undergoing scattering events have a strong probability of undergoing charge exchange processes with the surface [25]. The electron exchange processes generate secondary electrons which are necessary to sustain a plasma in glow-discharge sputtering [26]. The neutralization of the scattered ion may occur during incoming and/or outgoing trajectories but is considered to be most probable during the collision event [27].

Accurate estimates of ion reflection coefficients are difficult to measure experimentally due to neutralization processes but Eckstein and Verbeek [28] have estimated a value of 0.85 for 15 eV He^+ on tungsten and 0.4 at 4 keV. In the case of light ion reflection from compound targets, it is found that the reflection coefficient decreases relative to elemental scattering by a factor of around two [29].

2.4. Ion trapping

If the incident particle has sufficient energy to penetrate a surface, then entrapment may occur in the solid. In the case of light, inert, gases the entrapment will occur largely at lattice vacancies whilst for heavier ions non-substitutional dissolution may also occur [30]. The ion range in the solid depends strongly upon its energy and for energies greater than 10 keV, the implant depth can be accurately calculated [31]. An approximation is 1 nm keV^{-1}. At these energies the entrapment probability tends to unity. There is little experimental data for $E < 1$ keV, the range used in most deposition processes.

The theoretical predictions of low energy sputtering yields, ion reflection coefficients, entrapment probability and ion range are largely based upon computer models such at that of Biersack and Haggmark [32]. Typical range values for 500 eV O^+ in gold or ZrO_2 are 1.5 to 2.5 nm. For very low energy particles, 1 eV $< E <$ 200 eV, the surface trapping probability is close to unity so that the self-trapping coefficient of condensing atoms during film growth is close to unity.

The trapping probability $\eta(E)$ for inert gas projectiles behaves somewhat differently. Argon is frequently used as a support gas in many deposition processes and Carter and Armour [33] suggest that for many substrates $0.1 < \eta(E) < 1.0$ in the energy range 100 eV to 1 keV and $\eta(E) < 0.1$ for $E < 100$ eV.

Fig. 3 shows η as a function of Ar^+ and Kr^+ ion energy incident on borosilicate glass.

2.5. Ion-surface effects and film growth

The bombardment of the substrate by both energetic neutrals and ions will sputter clean the surface of impurities and absorbed gases. If reactive gases are present in large quantities during deposition the rate of absorbed gas evolution must be high enough to maintain a clean surface. The criteria for substrate contamination rate have been formalized by Carter and Armour [33].

For submonolayer gas adsorption ($n < n_s$) where n_s is the number of substrate atoms

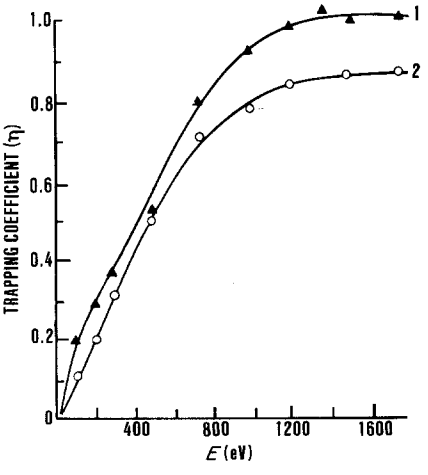

Figure 3 Entrapment probability as a function of incident (1) Ar^+ and (2) Kr^+ ion energy for glass targets [30]. Ion dose $D = 1.75 \times 10^{14}$ ions cm^{-2}.

$$\frac{dn}{dt} = k_p \gamma p\left(1 - \frac{n}{n_s}\right) - n$$
$$\left[\int_0^\infty \sigma_{d,c}(E)dJ_c(E) + \int_0^\infty \sigma_{d,s}(E)dJ_s(E)\right] - \frac{n}{\tau} \quad (4)$$

where k_p represent the molecular impingement rate per unit area at pressure p, γ the sticking coefficient, $\sigma_{d,c}$ the ion bombardment-induced desorption coefficient for coating species of flux density $dJ_c(E)$, $\sigma_{d,s}$ the cross-section for support gas particles, τ the residence time of adsorbed impurities before thermal desorption and $dJ_s(E)$ the flux density of support gas particles. An approximation for the equilibrium surface impurity is:

$$N_e \approx \frac{k_p \gamma p}{J\bar{\sigma}_d} \quad (5)$$

where J is the total flux. Under conditions of ion-plating, active gas pressures are about 10^{-2} Pa, and $k_p \approx 10^{19}$ atoms $m^{-2} sec^{-1}$. If $\bar{\sigma}_d \sim 10^{-19} m^2$ and the discharge current is 1 A m^{-2} (10^{21} particles $m^{-2} sec^{-1}$), then $N_e \sim 10^{13}$ atoms $m^{-2} \approx 10^{-2}$ monolayers. If impurities are recoil implanted with a cross section of $10^{-19} m^2$ impurity incorporation rate becomes $J\sigma_i N_e = 10^{19}$ atoms $m^{-2} sec^{-1}$, i.e. 1% of the coating atom arrival rate. These estimates show that for low impurity content of the growing films, low levels of residual contaminants in the vacuum system are necessary.

Low-energy ion bombardment of a growing film may be represented by the following expression [34]

$$I_i = J_i \Phi_i + \zeta_i \eta_i - \theta_i \Sigma_j (\zeta_j S_{ij}) \quad (6)$$

where I_i is the incorporation rate of a total flux; J_i the thermal component; ζ_i the energetic component, Φ_i the sticking coefficient of the thermal species, η_i the trapping probability of accelerated species, θ_i the steady-state surface fraction of species, ζ_j the incident flux of energetic species j and S_{ij} the effective sputtering yield of species i by species j. The third term accounts for the probability of species i being removed by self-sputtering from other accelerated particles of the same species or by bombardment from energetic, inert gas atoms reflected from a target surface. In the absence of ions Equation 6 reduces to $I_i = J_i \Phi_i$. When species i is accelerated as in reactive ion beam sputtering, $\zeta_i \eta_i$ is the dominant term. This approach is used to determine deposition rates, and average composition of films deposited under low-energy ion bombardment.

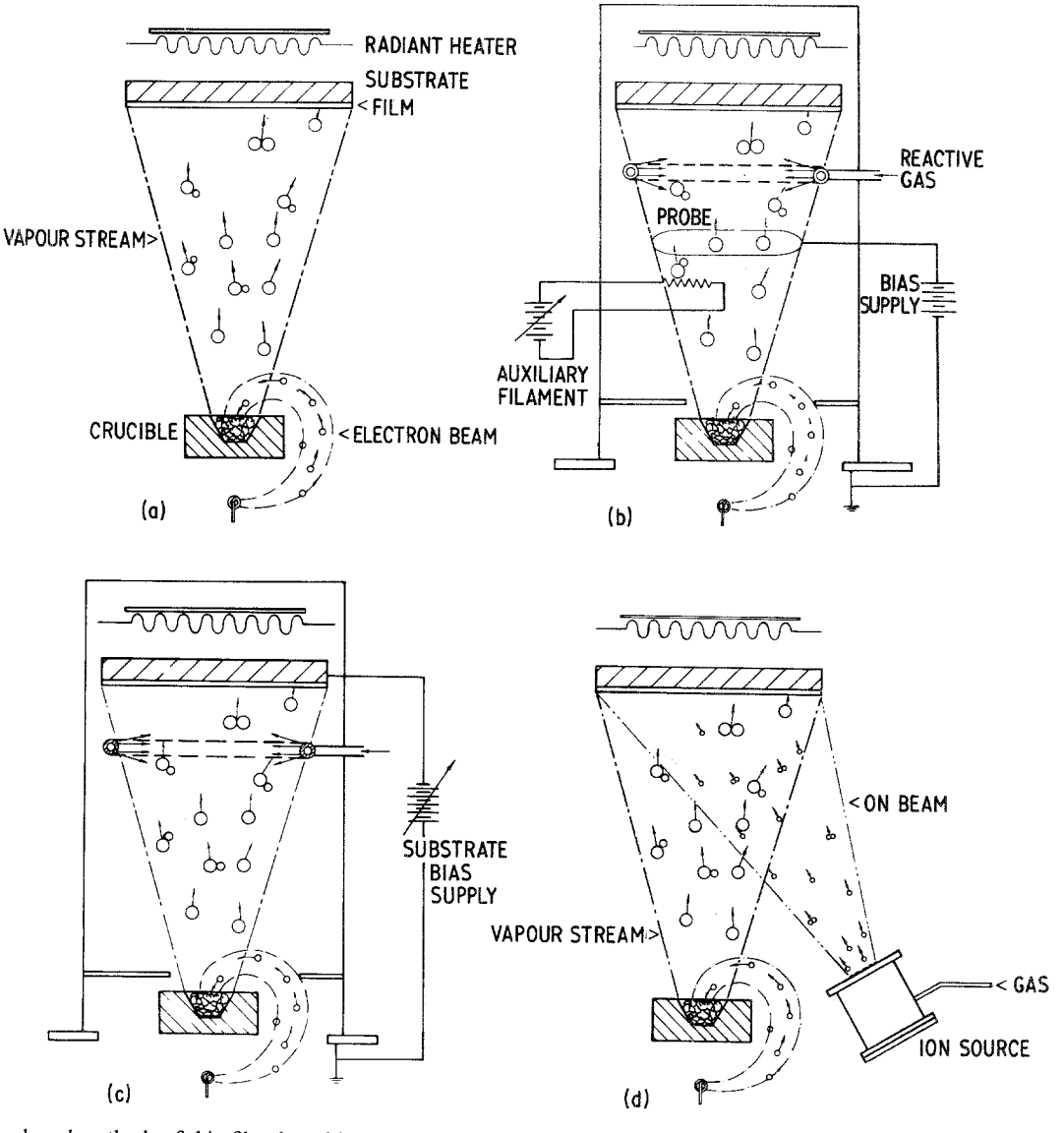

Figure 4 Ion-based methods of thin-film deposition (a) vacuum evaporation, (b) activated reactive evaporation (ARE), (c) ion plating, (d) ion-assisted deposition (IAD).

The relative importance of particle bombardment effects on growing films depends upon several factors, the major one being the particle energy. The particle energies are determined by the specific film deposition process employed, and the following section summarizes the most frequently used techniques.

3. Ion-based methods of optical thin-film deposition

3.1. Vacuum evaporation

In conventional evaporation the source material is heated until it evaporates and the vapour condenses on the substrate mounted directly above the source as shown in Fig. 4a. Electron-beam evaporation is more commonly used than resistance heating for greater control over source temperatures and deposition rates. The typical energy range of evaporated atoms is 10^{-2} to 1 eV and some ionization occurs through thermal dissociation and interaction with the electron beam. An ionized fraction of only 0.01% can influence thin film nucleation if accelerated to the substrate [35].

In oxide deposition evaporation can be performed in a background gas of oxygen at $\sim 2 \times 10^{-2}$ Pa. The technique is referred to as reactive evaporation and is often used to deposit compounds by promoting a reaction between evaporated metal atoms and the reactive gas [36]. Further control is possible by activating one of the species, for example by ionizing oxygen in an electrical discharge during titanium deposition. This method is termed activated reactive evaporation (ARE) and is shown in Fig. 4b. Deposition rates may be as high as several micrometres per minute in ARE, but by operating an auxiliary filament to sustain the discharge at reduced evaporation rates, the deposition rate may be made as low as 0.03 μm min^{-1} [37]. Ion-plating (Fig. 4c) is a further refinement of ARE where the substrate is biased negatively to attract positive ions formed in the electrical discharge. The benefits of ion bombardment during film growth can then be realized [38]. A particular advantage is that at high operating pressures the depositing atoms are scattered and the throwing power increased sufficiently to enable all exposed sides of the substrate to be coated [39].

3.2. Ion-assisted deposition (IAD)

The most significant advance in reactive evaporation technology has been the introduction of directed ion beams. Ionization of the residual gas increases the reactivity, and discharges (directed at a depositing film) were first tested by Heitmann [40]. The development of the Kaufmann-type ion gun [41] provided the necessary ion fluxes for practical deposition rates under low-energy ion assistance. With suitable modifications the ion-beam energy can be varied over the range 30 to at least 1200 eV [42]. Conventional electron-beam evaporation is improved by directing the flux from the ion gun on to the surface of the substrate and the growing film (Fig. 4d). For dielectric films the source is operated with oxygen gas to compensate for any preferential sputtering from oxide films [43].

3.3. Sputter deposition

Sputtering is attractive as a deposition technique since it is an atom-by-atom momentum transfer process. There is no direct heating of the material and no reaction between the evaporant and crucible as in thermal evaporation. Compounds and alloys are readily deposited and the geometry of the system is not limited to any direction. Sputtering may be ion-beam based (10^{-5} to 10^{-2} Pa) or plasma based (10^{-1} to 10 Pa). In ion-beam sputtering material is sputtered from a target and condensed on to the substrate as shown in Fig. 5. The Kaufman source is a suitable high flux ion gun for sputter deposition and films may be grown at a rate of about 1 μm h^{-1} depending upon the ion–target combination and geometry.

Dual-ion-beam sputtering is the sputter analogue of IAD. Weissmantel [44] demonstrated that structural and compositional modifications of the growing film could be achieved by irradiating the growing film with a second ion source. Diamond-like or i-carbon films were prepared as well as amorphous hydrogenated silicon, silicon nitride and cubic boron nitride.

Planar diode sputtering and magnetron sputtering are plasma-based sputter-deposition techniques (Fig. 6). Secondary electrons, created at the target surface by ion bombardment, accelerate and ionize the gas atoms to sustain a discharge. The applied power is

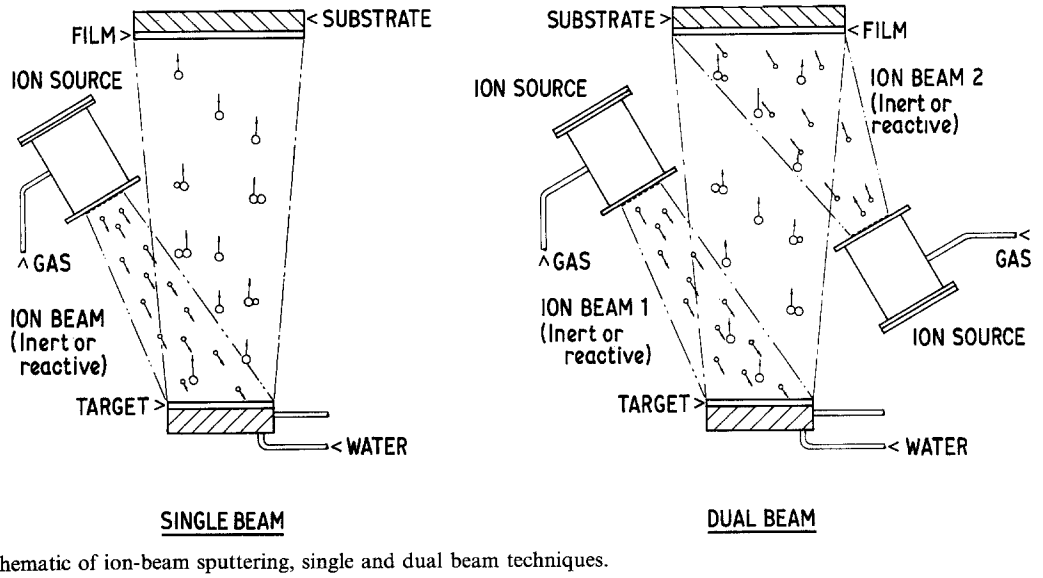

Figure 5 Schematic of ion-beam sputtering, single and dual beam techniques.

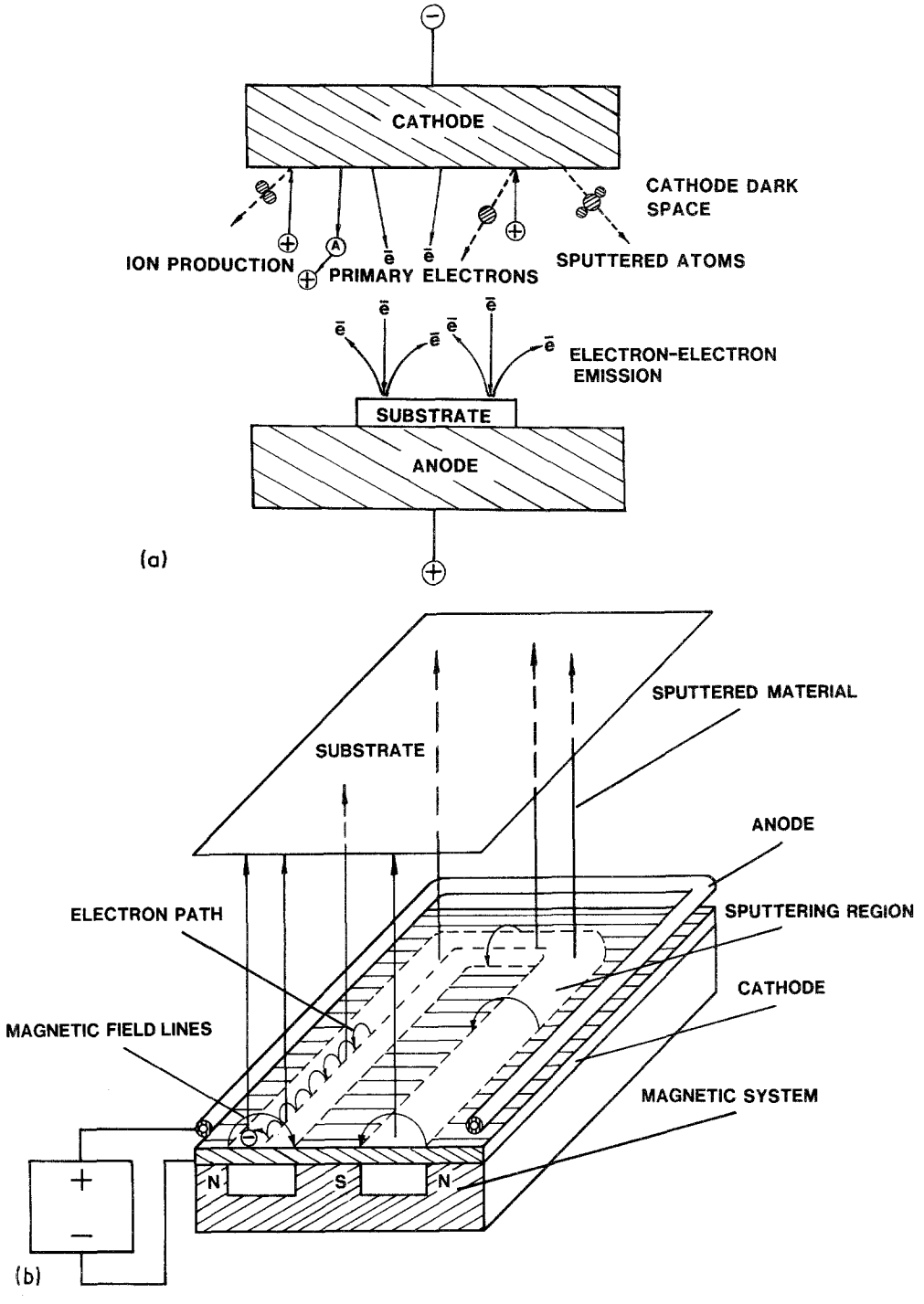

Figure 6 Schematic of (a) planar diode sputtering, and (b) magnetron sputtering.

generally d.c. for metals and r.f. for insulating targets. The working gas is typically argon but reactive gases are often used in combination or on their own for reactive sputter deposition of oxides, nitrides or carbides.

Magnetron sputtering is a means of achieving higher efficiency by confining the primary electrons to paths close to the cathode surface with applied magnetic fields. Ionization efficiency is improved and higher sputtering rates result [45–46].

3.4. Ion-beam deposition

This technique refers to a process in which the depositing atoms are fully ionized, accelerated, and deposited on a substrate as shown in Fig. 7. The deposition energy can be adjusted by substrate bias and substantial improvements in film properties have been reported particularly for diamond-like carbon films [47]. Although dense, hard, and highly-adhesive films with low stress have been deposited, the technique is restricted to low deposition rates.

4. Structure of thin films

The optical properties of films, such as refractive index, absorption, light scattering, and laser-damage threshold depend largely upon the film microstructure. The film material, substrate temperature, residual gas pressure and angle of vapour incidence can all influence the microstructure of optical thin films [48]. If the depositing vapour atoms have a low mobility on the substrate surface, three-dimensional island growth during nucleation and coalescence stages is promoted [49]. The film will then contain microvoids which may act as sinks for diffusing vacancies during and after

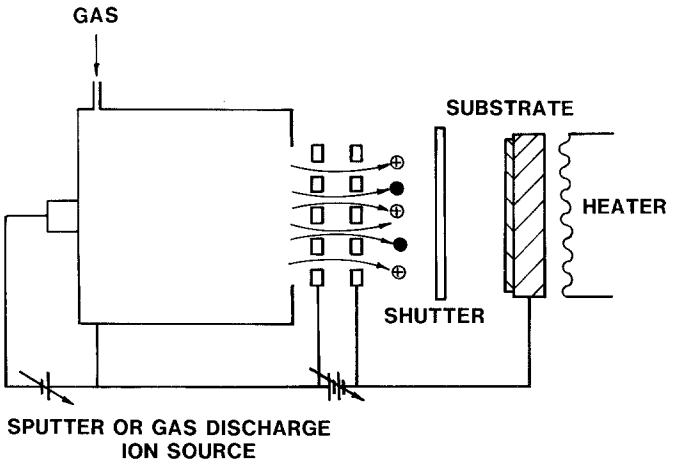

Figure 7 Ion-beam-deposition technique.

growth. Thin film microstructure is therefore of prime importance to optical performance and some control over its evolution during film growth highly desirable.

Thin film structures were first classified by Movchan and Demchishin [50] for thick metal and oxide deposits. In their scheme three characteristic structural zones were found which were determined by the substrate temperature, T, and the film material melting point, T_m. Zone I ($T/T_m < 0.25$–0.3) contained tapered columns with domed tops corresponding to low adatom mobility. In Zone II (0.25–$0.3 < T/T_m < 0.45$), a smooth topped granular structure is dominant and in Zone III ($T/T_m > 0.45$) equiaxial crystallites were formed with a polyhedral structure. The zone concept has been useful for classifying film structures since film mechanical properties are defined by the structural features of the relevant zone.

The zone concept was extended for sputtering conditions by Thornton [51, 52] who added a third coordinate to account for the influence of working gas pressure (Fig. 8). The zone structure was found to depend upon the interplay of atom shadowing, adatom diffusion, and surface and volume recrystallization. A macrostructure (open grain boundaries) results when adatom diffusion is insufficient to overcome shadowing effects and microstructure (closed-type grain boundaries) results from surface and volume recrystallization.

It has been proposed that the physical structure changes with film thickness. The evolutionary model of Messier *et al.* [53] is based upon an apparent repetition of honeycomb structures throughout the film thickness ($T/T_m \lesssim 0.5$). Conical-like columns evolve in a growth–death competition, their density determined by the size distribution of nucleating clusters on the substrate (Fig. 9).

Several authors have used computer simulation to study features of thin film nucleation and growth. Outlaw and Heinbockel [54] simulated the movement of surface atoms according to the influence of the interaction potential of the substrate and the lateral interaction of neighbouring atoms. Salik [55] found that a substantial fraction of clusters may be formed directly upon impingement and that surface migration and re-evaporation of atoms results in a decrease in the cluster density. Structural anisotropy and voids were modelled by Hendersen *et al.* [56] and their model modified by Kim *et al.* [57] to obtain more realistic film densities. The key feature of these early models was that evaporated individual spheres were deposited at random on the growing film and then allowed to relax to contact the nearest neighbours. The general features of film structure are then reproduced. Dirks and Leamy [58, 59] further refined the model by assuming the incoming molecule sticks immediately at its place of impact on the substrate with a probability of relaxing into the nearest triangular co-ordination location formed by two previously deposited atoms. The model predicts the formation of columnar growth, based upon self-shadowing, and the column orientation with respect to the substrate surface according to the tangent rule,

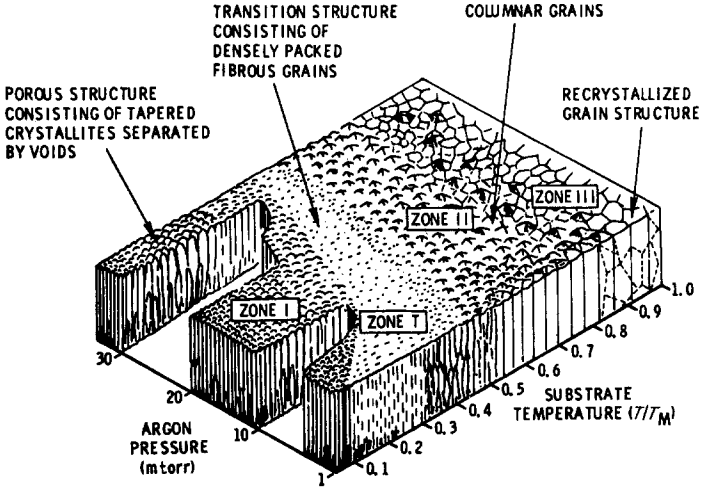

Figure 8 Three-dimensional zone-structure model [51].

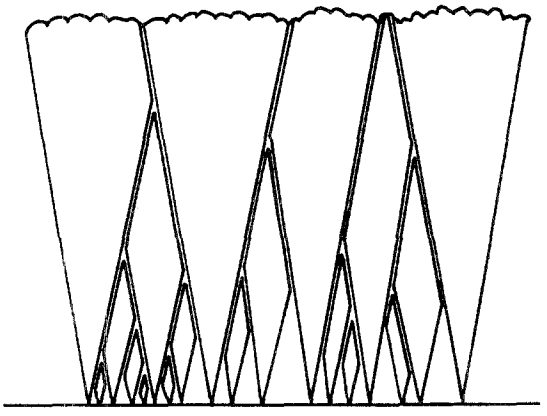

Figure 9 Fractal model of microstructure development [53].

$$\tan\alpha = 2\tan\beta \tag{7}$$

where α is the angle of the incident vapour stream and β the angle of inclination of the columns (Fig. 10).

Recently it has been shown by Müller [60] that the void density can be modified by simulating substrate heating during film growth or post-heating. An atom subject to a thermal fluctuation must overcome a threshold energy in order to jump from site β to neighbouring site β' given by,

$$\begin{aligned} \Delta E_{\beta-\beta'} &= (N'_\beta - N_\beta)\phi + Q \quad \text{if } N_\beta > N'_\beta, \\ &= Q \quad \text{if } N_\beta < N'_\beta \end{aligned} \tag{8}$$

where N_β, N'_β are the co-ordination numbers of two neighbouring sites, ϕ is the bonding energy and Q an activation energy. The hopping probability of an atom is determined by the vibration frequency $\nu_0 (\sim 10^{13}\,\text{sec}^{-1})$ and the sampling time per atom is given by,

$$\tau_s = \nu_0^{-1} \exp(Q/K\mathcal{T}) \tag{9}$$

The thermal energy fluctuation is given by,

$$\varepsilon = -KT \ln(1 - R)^\gamma \tag{10}$$

where $\gamma = \exp(-Q/K\mathcal{T})$ and the particle jumps when $\varepsilon > \Delta E_{\beta\to\beta'}$. Fig. 11a to d and 12a to d show the results of computer simulations for different temperatures at vapour flux incident angles of 30° and 60°. The first three atomic layers represent the substrate. In these simulations $Q = 0.7\,\text{eV}$ and $\phi = -0.7\,\text{eV}$. At low temperatures atomic shadowing leads to a porous columnar microstructure. As the temperature increases atom mobility is enhanced and the porous structure gradually disappears until the film packing density reaches a maximum. Fig. 13 shows the dependence of the film packing density on T for vapour flux angles of 30° and 60°.

The instability of optical coatings upon exposure to a humid atmosphere is largely attributed to thin film microstructure. Under typical deposition conditions (pressure 10^{-3} Pa, substrate temperature 30 to 300° C, rate 0.5 to 5 nm sec^{-1}) a dielectric film will generally develop columnar structure (Zone II type). Water from the atmosphere is then absorbed throughout the film by capillary action and the optical properties are then a composite of those of the film material and the absorbed water. The process is largely irreversible and has plagued optical film development for many years although attempts have been made to calculate the refractive index changes and distribution of pore sizes for a range of films [61, 62].

5. Ion bombardment effects on film properties

Many of the film properties are strongly influenced by changes in either structure or composition. The electrical properties of materials can be modified by doping with suitable impurities either by high energy ion implantation after film growth or by controlled doping during deposition [34]. Ion irradiation during film growth is a more effective means of controlling structure and/or composition over a greater range of film thickness than is possible by implantation.

5.1. Microstructure

One of the earliest demonstrations of film modification by ion bombardment was reported by Mattox and Komniak [63]. They deposited thick tantalum films by planar d.c. diode sputtering and also biased the substrate to attract positive ions. The application of bias was found to interrupt columnar growth and increase the film density close to the bulk value. The crystallite size also decreased with increasing ion bombardment. Similar effects were also observed during electron-beam evaporation by Bunshah and Juntz [64], who showed that a negative substrate bias attracted

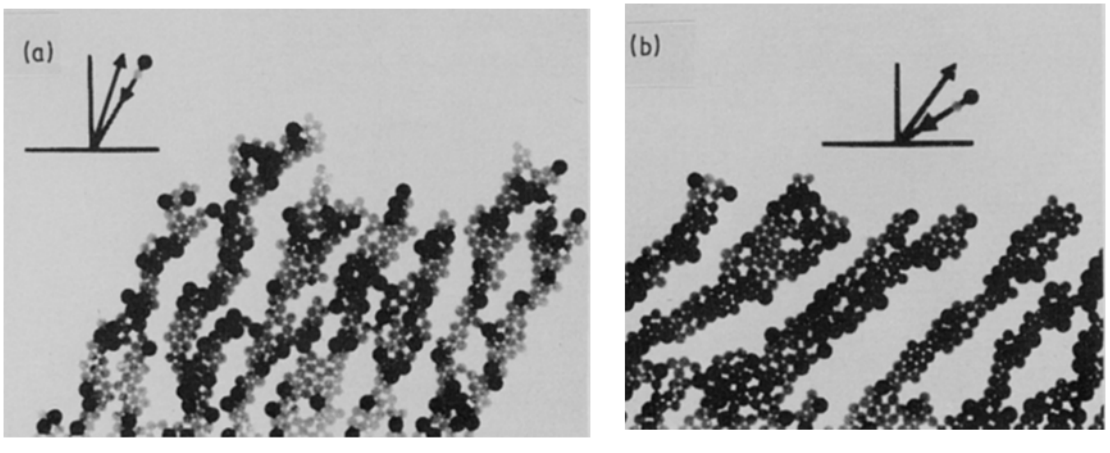

Figure 10 Computer simulation of an $A_{0.2}B_{0.8}$ hard disk alloy "deposited" at (a) $\alpha = 30°$ and (b) $\alpha = 60°$ [58].

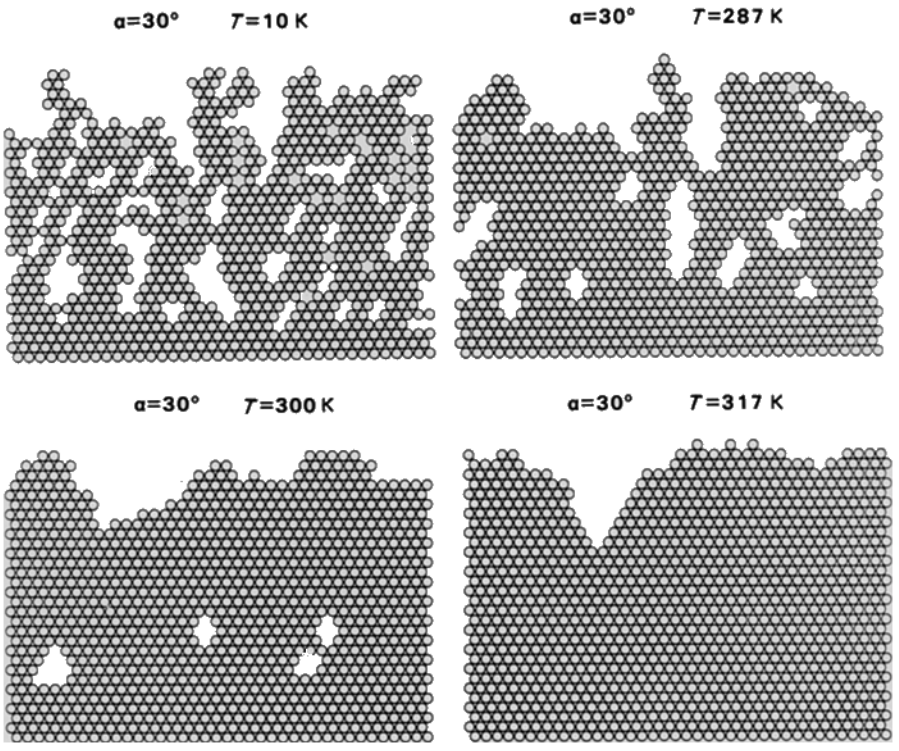

Figure 11 Computer simulation of the effect of substrate temperature on the void density of growing thin films for vapour incidence angle of 30° [60].

positive ions and refined the grain structure of the growing films.

Monoenergetic ion sources have also been used to irradiate growing films [65–67]. In general, metallic films exhibit preferred orientation in their crystal structure. These effects are attributable to the focusing of collisions along preferred directions in the film and the channelling of the incident particles [68]. Babaev *et al.* [69] found that ion bombardment also causes the development of nucleus orientation which is enhanced by substrate orientation, and accelerates film growth.

The effect of ion bombardment on the microstructure of growing films [43] can be seen from comparisons of spectral transmittance curves of layers immediately after deposition and on venting to a humid atmosphere, as shown in Fig. 14. The effect of water absorption into the voids of columnar films prepared without ion assistance can be seen by the shift of the curve to longer wavelengths. Densely packed ion-assisted optical films which do not absorb water vapour were first reported by Martin *et al.* [70]. Dense oxide films of silicon, titanium and zirconium were prepared with argon-ion assistance. The density of ZrO_2 films was improved by both argon and oxygen ion-assisted deposition [43].

Direct observation of the microstructure of dielectric

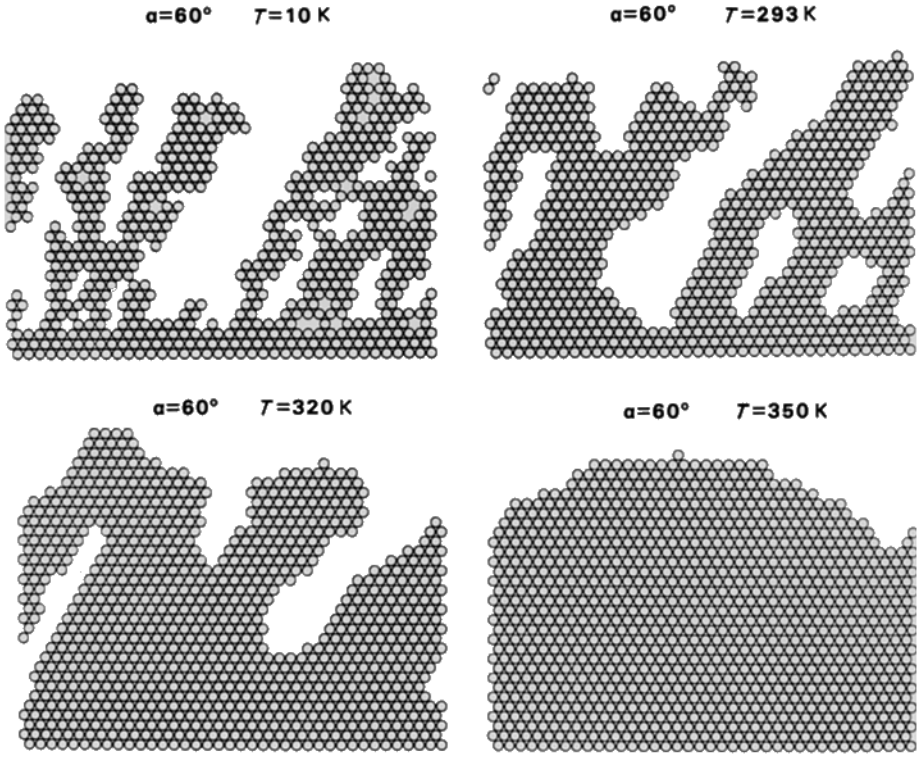

Figure 12 Computer simulation for vapour incidence angle of 60° [60].

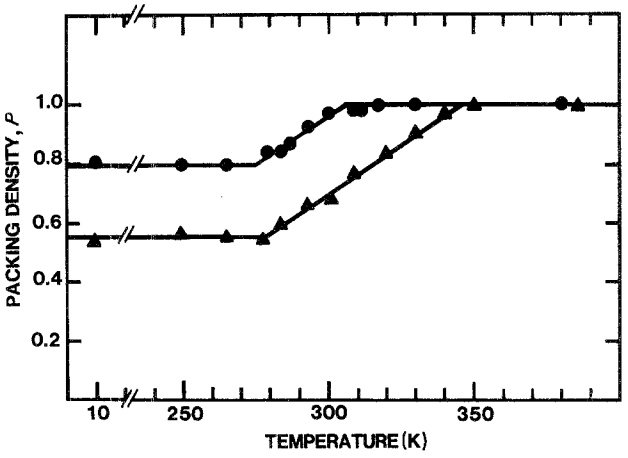

Figure 13 The calculated dependence of film packing density on substrate temperature for vapour flux angles of incidence of (●) 30° and (▲) 60° [60].

films by scanning electron microscropy is difficult and a conducting coating such as gold must be applied to prevent charging by the electron beam. Replication transmission electron microscopy techniques must be used for high resolution work [48]. Fig. 15 shows the typical microstructures observed in optical multilayers produced by evaporation. Pronounced columnar structure is evident in the TiO_2 layers but not in SiO_2 layers. The effect of ion bombardment on microstructure modification is readily seen in Fig. 16 of thick TiN films prepared with and without substrate bias during sputtering [71]. The mechanisms responsible for film densification by ion bombardment have yet to be positively identified but must include local resputtering, recoil and cascade mixing and to some degree thermal and/or displacement spikes.

5.2. Film composition and compound formation

Dudonis and Pranevicious [72] showed the influence of oxygen-ion bombardment on the properties of vacuum-evaporated thin films. Aluminium amd silicon monoxide were evaporated by electron-beam heating at a constant rate of 0.5 to 2 nm sec^{-1} and when bombarded with 5 keV oxygen ions Al_2O_3 and SiO_2 oxides were formed at doses of 10^{21} and 10^{23} ions cm^{-3}. The refractive index of SiO_2 films could be varied with ion dose as shown in Table II [73]. Aluminium nitride was also synthesized by aluminium evaporation and nitrogen ion irradiation.

The bombardment of a continuously deposited film by reactive or inert-gas ions in a reactive-gas atmosphere stimulates a surface chemical reaction. Grigorov *et al.* [74] observed that the capture coefficient and sorption ratio of depositing titanium films was increased sevenfold by 1 keV Ar^+ irradiation in a nitrogen atmosphere. Super-stoichiometric films of TiN_x where $x \gtrsim 1.15$ were reported. The increase in the capture coefficient was correlated with the number of vacancies and interstitials generated at the growth surface by radiation damage.

The irradiation of growing oxide films with nitrogen beams has also been successful in synthesizing oxynitride films [75].

5.3. Adhesion and stress

A comparative study of gold films prepared by various deposition methods by Chopra [76] revealed that sputtered films were more adherent than evaporated films and that the adhesion was independent of the deposition rate. Adhesion is sensitive to the state of the substrate–film interface and is generally improved if the average arrival energy of depositing atoms is increased. Since sputtered atoms have between 10 and 20 times greater energy than evaporated atoms, it is to be expected that secondary sputtering of substrate contaminants and some degree of atomic mixing at the interface will occur. In some systems the use of an oxygen-ion beam during nucleation and growth stages can considerably enhance the film adhesion by chemical effects [77].

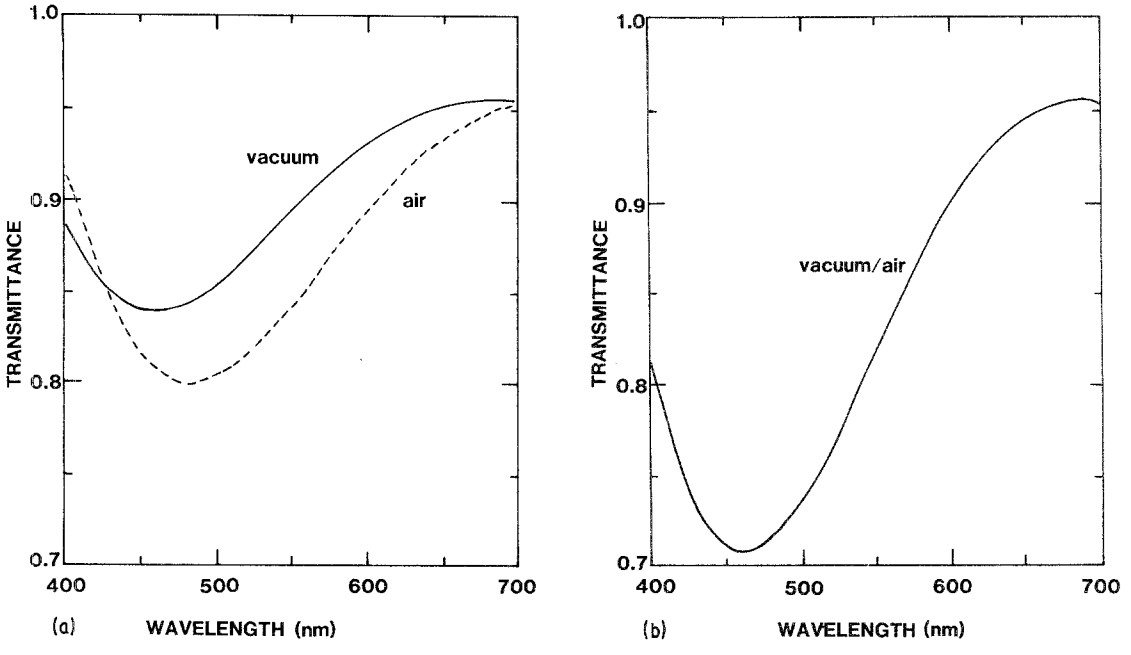

Figure 14 Transmittance over the visible spectrum of a ZrO_2 film deposited (a) without ion-assistance and (b) with oxygen-ion assistance. Solid line is vacuum data and broken line in air [43].

TABLE II Dependence of the refractive index of SiO films on the concentration of implanted oxygen [73]

C (cm^{-3})	0	2×10^{19}	2×10^{22}	6×10^{22}	1×10^{23}
n	1.85	1.86	1.55	1.48	1.46

TABLE III Optimum conditions for the kinetic energy of ions incident on the substrate for film formation [80]

Condition	Required incident ion energy	Result
Deposition	Less than the energy corresponding to the sputtering rate, $S(E) = 1$. Larger than the energy at which the sticking probability becomes too low	
Surface cleaning	Larger than the energy of adsorption on the substrate surface, i.e. 0.1 – 0.5 eV for physically adsorbed gases and 1 to 10 eV for chemically adsorbed	→ Optimum value of kinetic energy: a few to a few hundred electronvolts
Good quality film formation	In a range where enhanced adatom migration influences properties of the deposited film suitable ion bombardment affects the growth of nuclei. A suitable amount of defects or atomic displacement near the substrate surface contributes to film formation during the initial stage	

Both adhesion and stress may be modified by ion-assisted deposition. Hirsch and Varga [78] reduced the stress of thick germanium films and Cuomo *et al.* [79] modified the stress of niobium films from tensile to compressive by means of argon irradiation.

5.4. Summary

The general requirements for optimum film growth in terms of the kinetic energy of ions present have been summarized by Takagi [80] (Table III). The kinetic energy of ions is converted to; (1) sputtering energy, (2) thermal energy, (3) implantation energy, (4) migration energy on the substrate surface, and (5) creation energy of activated centres for nucleus formation. Furthermore, ions of very low energies may still influence film nucleation and growth and enhance chemical reactivity.

6. Optical properties of thin films

Ion-based thin-film deposition techniques are used to deposit materials for a wide range of applications. We restrict ourselves in this review to those materials which find their greatest application in optical devices. Dielectric oxide films are an important class of materials since they form the basis of most thin-film filters and, therefore, are discussed in some detail. Carbon films are presently being studied by many researchers and show great promise for many optical applications because of their very attractive properties and are also briefly discussed.

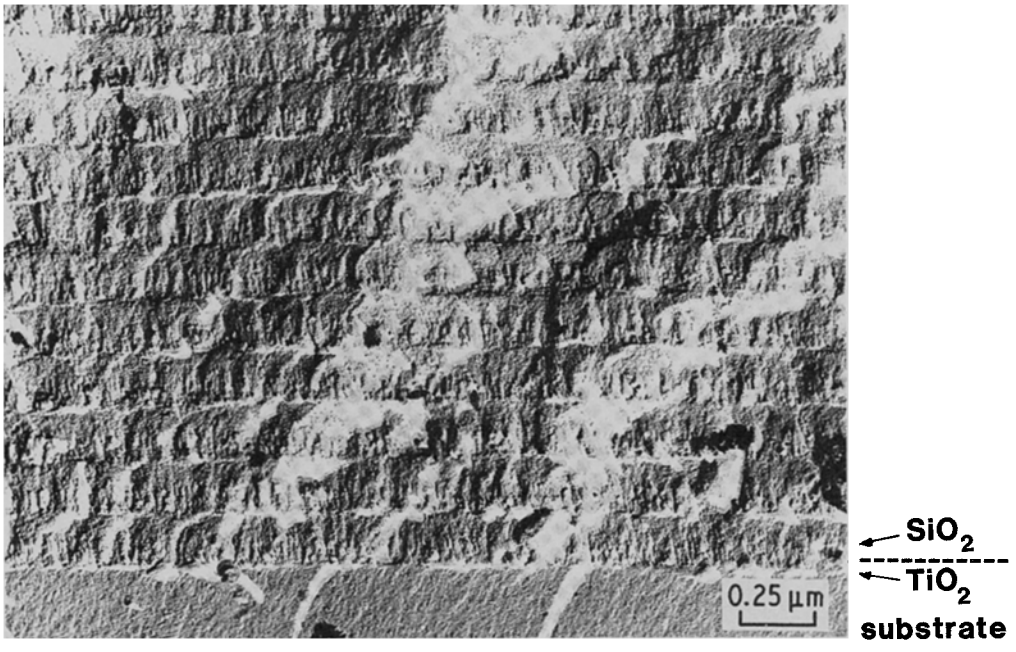

Figure 15 Microstructure of a thin film multilayer of alternating SiO_2 and TiO_2 layers. Columnar structure evident in the TiO_2 layers is not seen in the SiO_2 layers [48].

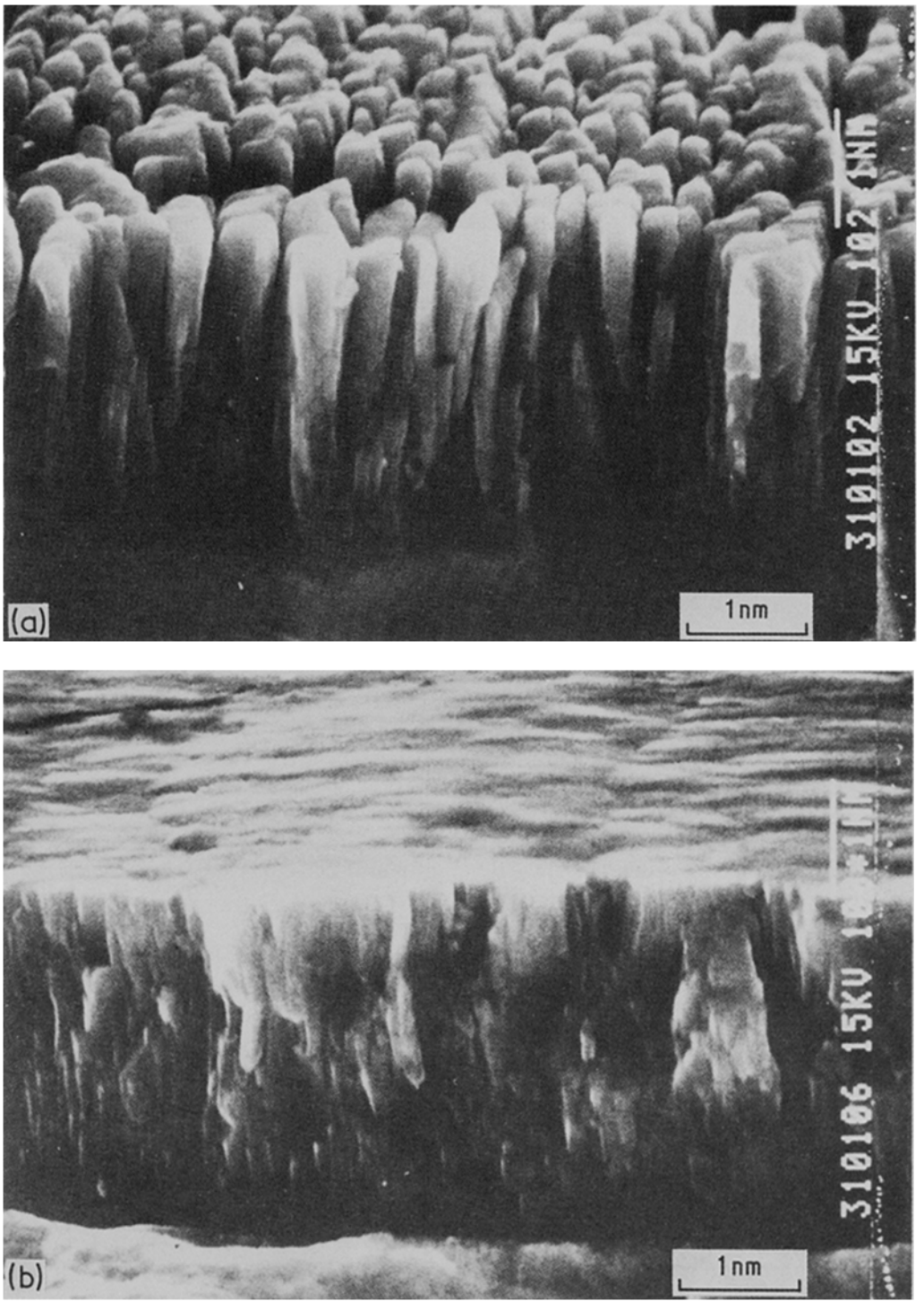

Figure 16 Gross columnar structure observed in TiN films deposited (a) by magnetron sputtering and (b) the reduction of columnar growth by bias-deposition i.e. deposition under ion bombardment [71].

6.1. Silicon dioxide

Silicon dioxide is the material most frequently used in combination with TiO_2 in multilayer interference stacks and is also an important dielectric in the electronic industry. Consequently this material has been prepared by various techniques extending from simple evaporation of silica to oxygen ion-implantation into silicon [81]. A number of problems are associated with silica deposition, i.e. porous films, variable index, and substrate temperature effects. When SiO_2 is deposited by evaporation as an alternating layer with TiO_2, electron-microscopic observations reveal that the gross columnar structure always observed in TiO_2 is absent in the SiO_2 layer (Fig. 15). The low packing density of SiO_2 is influenced to a small degree by substrate temperature. Deposition in ultra-high vacuum by electron-beam evaporation yields packing densities of 0.95 and 0.99 at substrate temperature of 50 and 250° C respectively [82]. Reale [83] reports values of 0.88 and 0.98 at the same temperatures. Heitmann [75] has measured a value of 0.93 for films deposited at room temperature by low-energy IAD. We see, therefore, that unity packing density is not achieved even at relatively high substrate temperatures.

The effect of ion species and ion flux on the refractive index for IAD Silica, SiO_2 starting material [84, 85], is shown in Fig. 17. The refractive index increases

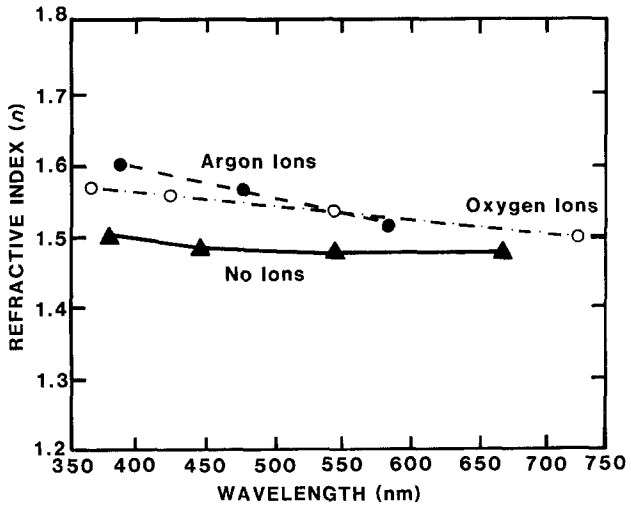

Figure 17 The influence of ion species on the refractive index for IAD silica [85].

due to the packing density modification for both argon and oxygen ion bombardment relative to conventionally deposited silica (no ions). The extinction coefficient was too low to measure at 550 nm. Absorptance at 1.06 μm was also very low (9×10^{-6}) increasing to 2.1×10^{-5} at 325° C substrate temperature for a 345 nm thick film. The effects of oxide reduction due to preferential sputtering, which increases absorption in TiO_2, was not observed for silica films and was attributed to the stronger chemical bond between silicon and oxygen atoms.

Sputter deposited films do not exhibit significantly different refractive indices to conventionally evaporated films [86]. Fig. 18 summarizes the optical measurements reported for ion-based silica deposition. The values vary considerably for most wavelengths from the bulk silica curve, although many authors routinely report 1.46 for n at 550 nm.

6.2. Aluminium oxide

Aluminium oxide is also an important material in the electronics industry where it is used as a passivating layer in metal-oxide/semi-conductor devices and thin dielectric films in integrated circuit applications. It is also extensively used in optics as a protective film for metal reflectors, multilayer applications, and solar selective surfaces. The material can be deposited by most techniques, and variations in properties are to be expected since nine phases of aluminium oxide are listed in the ASTM powder diffraction file. Of the seven evaporated materials studied by Reale [83], Al_2O_3 had the highest packing density of 0.95, showed the least variation with substrate temperature, and had a constant refractive index of 1.60 up to a substrate temperature of 300° C. Both r.f. and d.c. sputtering techniques are used in Al_2O_3 deposition. Adherent amorphous films were deposited to a thickness of 8 μm at 40 nm sex^{-1} by Nowicki [87] by r.f. planar magnetron methods. The film stoichiometry was dependent upon the power density and approached Al_2O_3 at 4 W cm^{-2} giving a refractive index of 1.63 at 546.1 nm. The Al_2O_3 targets were sputtered using pure argon and the films contained argon up to a maximum of 4.8%. No details of film absorptance were given in this work but absorptances of less than 1.0% in films prepared by d.c. magnetron sputtering of aluminium in a 10% oxygen–argon mixture have been reported [88].

Pawlewicz *et al.* [86] have reported a mid-range index of 1.67 for Al_2O_3 prepared by r.f. diode sputtering of aluminium in argon–oxygen mixtures. The films were thought to be stoichiometric and the structure cubic. The refractive index was also found to be 1.67 at 1.06 μm.

Ion-assisted deposition has also been used [89, 90], and a refractive index of 1.65 at 633 nm and an extinction coefficient of 1.8×10^{-6} were reported.

The dispersion of the refractive indices reported for some recent studies of Al_2O_3 is shown in Table IV.

6.3. Titanium dioxide

Titanium dioxide is a hard, chemically resistant material, transparent in the visible and near infrared and with a high refractive index. Consequently this material is widely used in thin-film technology and has been deposited by a range of techniques. Titanium dioxide occurs in three main crystalline forms, rutile, anatase and brookite, although the latter has not been observed in vacuum deposited thin films. The phase diagram of the Ti–O system of Roy and White [91] shows there exists an indeterminate number of phases between TiO and TiO_2, of which Ti_2O_3 and Ti_3O_3 and Ti_3O_5 are the distinct phases and TiO_2 (anatase) is the

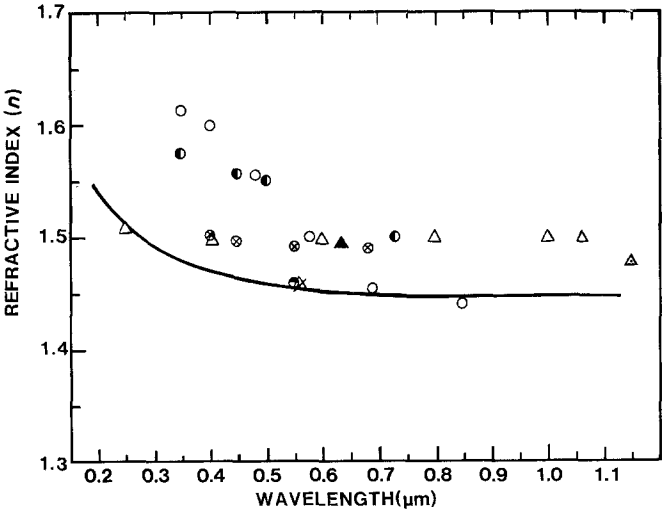

Figure 18 Summary of the refractive index as a function of wavelength of SiO_2 prepared by ion-based techniques. Solid line is silica data. Various methods; IAD, ○ [84] ◐ [85], ◓ [89]. Evaporation, ⊗ [85]. Sputtering, ▲ [97], △ [86] △ [115], △ [105].

TABLE IV Refractive indices of Al_2O_3 films produced by ion-based techniques

Wavelength λ (μm)	Refractive index n	Reference
0.25	1.70	86
0.30	1.70	86
0.40	1.70	86
0.50	1.70	119
0.54	1.63	87
0.55	1.63	86
0.60	1.68	86
0.63	1.65	114
0.80	1.68	86
1.00	1.64	119
	1.67	86
1.06	1.67	86
5.00	1.74	

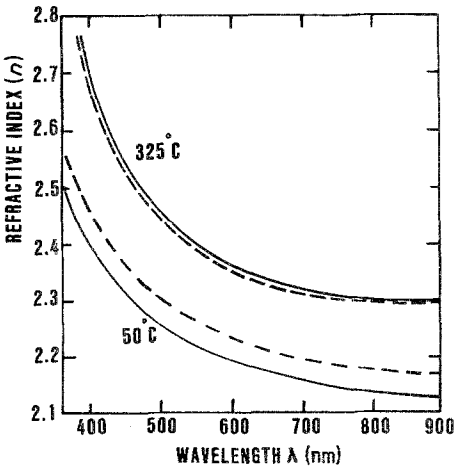

Figure 19 The deposition of TiO_2 indices for the starting materials — TiO_1 and — — — Ti_2O_3 at substrate temperature of 50 and 325° C [99].

stable oxide phase at a temperature of 400° C [92]. The most desirable oxide phase from the point of view of optical properties is rutile. It is then not surprising that the substrate temperature and the degree of oxidation of the film are critical parameters for TiO_2 deposition, and that the optical properties obtainable will vary from technique to technique. A comprehensive study of reactive evaporation methods by Pulker *et al.* [93] has highlighted the problems encountered in TiO_2 deposition by conventional techniques. The refractive index is dependent upon the substrate temperature, the oxygen partial pressure during deposition, and the deposition rate. Successive evaporation of different starting materials results in different refractive indices of the deposited films, particularly for TiO, Ti_2O_3 and TiO_2 starting materials. Reproducible results were obtained only when Ti or Ti_3O_5 starting materials were reactively evaporated. The variations in index with successive evaporations of the other source materials is attributable to their changing composition in the crucible during deposition, which in turn results in a varying vapour stream composition.

A major problem, however, with reactive evaporation is the reduced packing density of the deposited material, a parameter which can only be influenced by depositing at elevated substrate temperatures in order to enhance surface mobility of depositing atoms and molecules. Grossklaus and Bunshah [94] have prepared rutile by reactive evaporation but at very high oxygen partial pressure and elevated substrate temperatures of up to 1100° C.

Higher packing densities are achieved by sputtering techniques where greater mobility of surface atoms is possible due to their higher deposition energies. Considerable control over the oxide phase and grain size has been achieved by r.f. sputtering [95, 96]. Rutile is obtained over a wide range of temperatures at high oxygen pressures and the corresponding grain size varies from 10 to 60 nm. The influence of grain size on the refractive index is difficult to separate from packing density effects but is reported to increase n by approximately 5% [96].

In general, sputtering is the preferred method for depositing TiO_2 with reproducible properties, although good results have been obtained using reactive r.f. biased ion plating. Using this technique Suzuki and Howson [97] have obtained high quality TiO_2 films (n = 2.49 at 633 nm) on water cooled glass substrates. However, the refractive index is sensitive to the deposition rate and oxygen partial pressure. TiO_2 was also prepared by d.c. magnetron sputtering and r.f. enhanced d.c. magnetron sputtering. In the latter technique, r.f. bias is applied to the substrate. An advantage of these techniques is that the source material can be titanium which is sputtered at a relatively high rate.

Ion beams have been used by Takiguchi *et al.* [98] to deposit titanium oxides directly by sputtering metal targets in oxygen, but the most successful application has been in ion-assisted deposition (IAD). Heitmann [75] evaporated Ti_2O_3 with oxygen-ion assistance. At 550 nm, the refractive index was estimated to be between 2.2 and 2.3 and found to depend slightly on deposition rate. The absorption coefficient at 633 nm was estimated to have an upper limit of 40 cm^{-1}, and at 10.5 μm was 10^3 cm^{-1}. Single crystal rutile reaches a comparable absorptance only at 11.6 μm. The discrepancy was assumed to be a structural effect as the IAD films were all amorphous.

The experiments of Heitmann were later repeated in greater detail with a refined Heitmann ion source [89, 99]. Both TiO and Ti_2O_3 materials were used and the effect of neutral oxygen, positive and negative ions, and excited molecules on the absorption and refractive index investigated over the substrate temperature range 50 and 325° C. The data are summarized in Fig. 19.

Further demonstrations of the success of IAD were made by Allen [84] with negative ions (and electrons) and TiO as the starting material. The absorption coefficients at 1.06 μm obtained are given in Table V.

TABLE V Measured absorptance at 1.05 μm of reactively deposited titania films as a function of source current [84].

Source current (mA)	Measured absorptance, α	Absorption coefficient (cm^{-1})
150	1.9×10^{-1}	1992
250	1.8×10^{-3}	29
350	9.0×10^{-3}	160

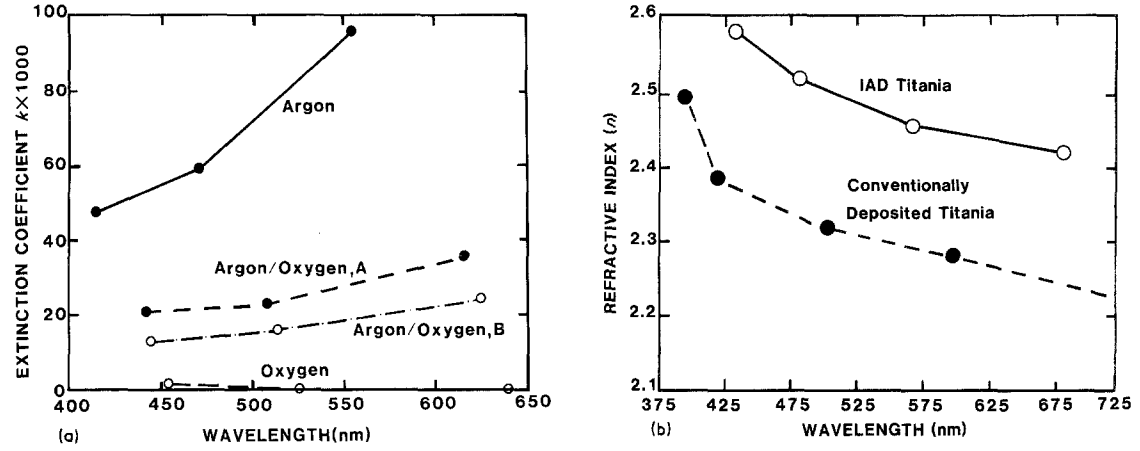

Figure 20 (a) Variation of the extinction coefficient of titania using argon, oxygen and mixed ions. E(argon) = 400 eV, γ = 1.7; E(argon/oxygen, A) = 400 eV, γ = 0.17; E(argon/oxygen, B) = 300 eV, γ = 0.12; E(oxygen) = 300 eV, γ = 0.12. γ is ion to molecule ratio at the substrate [85]. (b) Comparison of the refractive indices of IAD and conventionally deposited titania films E(oxygen) = 300 eV, γ = 0.12 [85].

X-ray diffraction measurements also revealed these films to be amorphous.

Allen [85] has recently studied the influence of 300 and 400 eV argon and oxygen positive ions with a Kaufman ion source. Fig. 20 shows the effect of the ion bombardment on the optical properties for different ion-to-TiO molecule ratios at the substrate. The best results were found for oxygen bombardment where very low values of the extinction coefficient k were obtained. Absorptance figures at 1.06 μm are shown in Table VI. Titania films were found to have the lowest absorptance using 300 eV oxygen ions at an ion-to-molecule ratio of 0.12 which yielded a refractive index of 2.49.

The effect of low energy bombardment on optical properties has been studied by McNeil *et al.* [100]. The film absorptance is reduced for the lower energy case although no figures on index or absorptance were given. It was found that the ion bombarded films had considerably less hydrogen and hence less water vapour penetration than films deposited without ions.

All IAD studies of titania have shown that the deposited films are amorphous. These observations are consistent with earlier studies of bombardment-induced structural changes in solids. Furthermore, a TiO_2 sample subjected to an intermediate ion dose (10^{17}–10^{20} ions m^{-2}) will revert to the lower oxide Ti_2O_3 [17]. Since film growth is essentially a layer by layer process, and each layer ion bombarded, the situation is equivalent to post-bombardment of bulk oxides.

The dispersion of the refractive index of TiO_2 that may be obtained by the various techniques is summarized in Fig. 21. It is interesting to note that there is a considerable spread in data points and very few results approach the optical properties of bulk rutile. IAD data points show a good reproducibility between various groups, but in general fall short of the rutile values at most wavelengths. All the IAD data was taken from samples deposited on unheated substrates which generally leads to inhomogeneous coatings in conventional evaporation. The IAD data is, however, in good agreement with that of Chereponova and Titova [101] for TiO_2 films deposited by evaporation on substrate maintained at 300° C, indicating that ion-assistance is equivalent to enhancing film atom mobility by substrate heating.

TABLE VI Variation in absorptance at 1.06 μm with various source gases [85]

Source gas	Absorptance α $\alpha \times 10^{+6}$
Argon	319 000
Argon and oxygen	65 000
Argon and oxygen	41 300
Oxygen	514

6.4. Zirconium dioxide

This material also has a high refractive index and is hard but is subject to considerable variation of refractive index with deposition conditions [102, 103]. The packing density of ZrO_2 is considerably less than that of other dielectrics when deposited by evaporation. Reale [83] gives a figure of 0.7 at 50° C and 0.95 at 300° C substrate temperature with a corresponding rise in index from 1.80 to 2.15. Perveev *et al.* [104, 105] report a 12% porosity for evaporated ZrO_2. With such a poor packing density it is not surprising that wide variations in optical properties are reported.

The growth of ZrO_2 can be substantially influenced by ion bombardment. Greene *et al.* [106] showed that r.f. bias-sputtered Y_2O_3-doped ZrO_2 films are modified by increasing the bias from −40 to −80 V. The −40 V biased specimens exhibited columnar microstructure but when the bias was increased to −60 V the columnar structure was removed. The oxygen/zirconium ratio was also increased by increasing the bias. Pawlewicz and Hays [107] examined the microstructure of various ZrO_2 films prepared by r.f. sputtering also as a function of bias. The predominant crystal structure of ZrO_2 films prepared by sputtering zirconium in argon–oxygen mixture is monoclinic. At target power densities higher than 10 W cm^{-2} the substrate temperature increased to 750 K and the crystal phase changed from monoclinic to tetragonal. The cubic phase was observed for CaO and Y_2O_3 doped ZrO_2 films prepared with no bias. Bias sputtering of

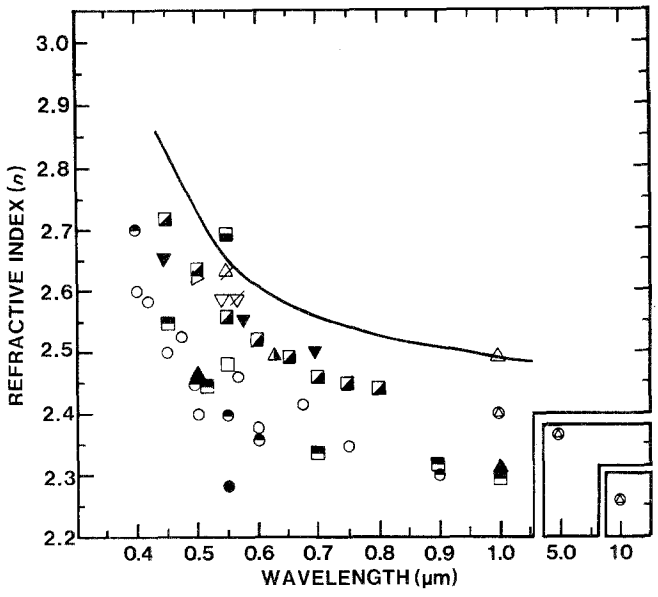

Figure 21 Summary of the dispersion of the refractive index of TiO_2 produced by ion-based techniques. Solid line is the bulk rutile data. Various methods; IAD, ● [75], ○ [84], ◐ [85], ◓ [89]. Sputtering, △ [86], ▽ [96], ▲ [97], ⧋ [104], ▼ [115], ◬ [117], ⧩ [118], ▲ [119], ◍ [146]. Reactive evaporation, □ [82], ◪ [93], ▣ [101], ▬ [116].

ZrO_2–CaO results in preferential sputtering of calcium and a change back to a monoclinic phase.

A detailed study of the modification of the optical and structural properties of dielectric ZrO_2 produced by ion-assisted deposition has been made by Martin *et al.* [43]. The effect of ion irradiation on the optical properties is most clearly demonstrated by the observation of vacuum–air effects due to water absorption as shown in Fig. 14. Stable films which did not adsorb water were produced for a ZrO_2 arrival-rate-to-ion-flux of 3.5 for 1200 eV O_2 ions. The results are interpreted as absorption by capillary-action of water vapour into the microvoids of the low-packing-density films, resulting in a change in the film refractive index.

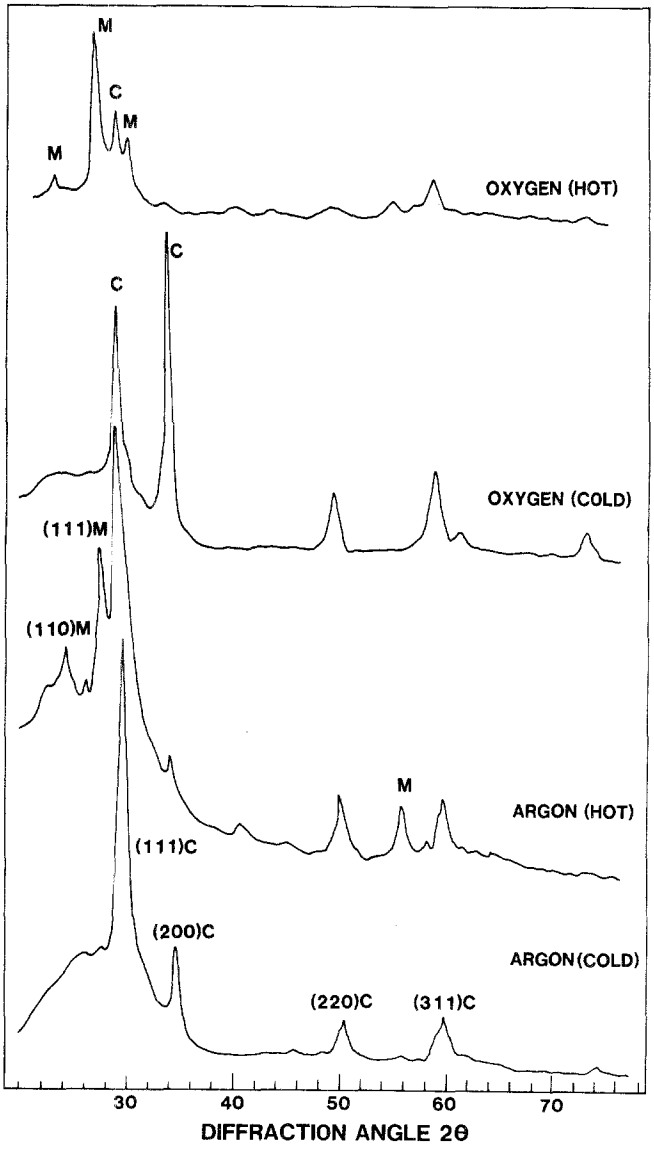

Figure 22 X-ray diffraction spectra for ZrO_2 films produced by argon and oxygen IAD on room temperature and heated substrates [43].

Ion-assisted deposition increases the packing density and prevents water penetration. Evidence for this mechanism was provided by profiling the films for water vapour and detecting hydrogen (from water vapour) as a function of film thickness by nuclear reaction analysis. A substantial reduction in hydrogen, and hence water vapour content, was seen for ion-assisted films.

The crystal structure of ZrO_2 is considerably modified by ion-assisted deposition. Films deposited at room temperature in the absence of ions show no X-ray diffraction lines. However, ion irradiation produces a face centred cubic structure when the ion current density is greater than $5 \times 10^{-2} A\,m^{-2}$ (ion: atom arrival rate 1 : 75, Fig. 22). Heated films exhibit only the monoclinic phase in the absence of ions but both a cubic and monoclinic phase in the presence of ions. The ion-induced crystallization effects closely follow the observations for post-irradiation of amorphous ZrO_2 by 2 to 35 keV Kr^+ [17], where ion impact promoted a crystallization of the cubic phase.

It is not possible at this stage to attribute the main crystallization mechanisms in IAD processes to spike effects as suggested in [17], but simple heating processes are not thought to be significant. The amorphous-cubic phase transition temperature for ZrO_2 is 400° C [108], which is far greater than the substrate is likely to achieve from simple radiative heating from the crucible during deposition.

The changes in crystal structure and film packing density have a strong influence on the optical properties of ZrO_2. Fig. 23 shows the refractive index at 550 nm as a function of argon and oxygen ion current density. For argon, a vacuum–air shift is observed up to an index of 2.138 and then the refractive index decreases. This index reduction at high argon current densities is due to preferential sputtering of oxygen and argon incorporation into the layer. Films produced by oxygen bombardment are much more stable and a maximum index of 2.19 is achieved. The highest indices for both ion species are observed only when the substrate is heated and the film is ion bombarded.

An interesting effect was also found on the optical properties when the ion beam was switched either off, or on, during a deposition. Fig. 24 shows the transmittance at 550 nm as a function of film thickness. In case (a) the film is deposited with oxygen ions and an index of 2.18 was measured. The deposition continued with the ion flux switched off resulted in a reduced index of 1.9. The reverse case – no ions then ions on – almost reproduces the results in reverse. Ion-assisted deposition is shown to produce an immediate effect on the packing density of ZrO_2 and is sufficient to disrupt columnar growth even on a low packing density layer under continuous deposition condition.

The available data on the refractive indices of ZrO_2 are summarized in Table VII.

6.5. Cerium dioxide

Cerium dioxide has been prepared by sputtering and ion-assisted deposition [109, 110]. As with other oxides prepared by IAD, vacuum–air changes in the refractive index are observed until the ion current density reaches an optimum value. Fig. 25 shows the index behaviour for oxygen bombardment. A gradual

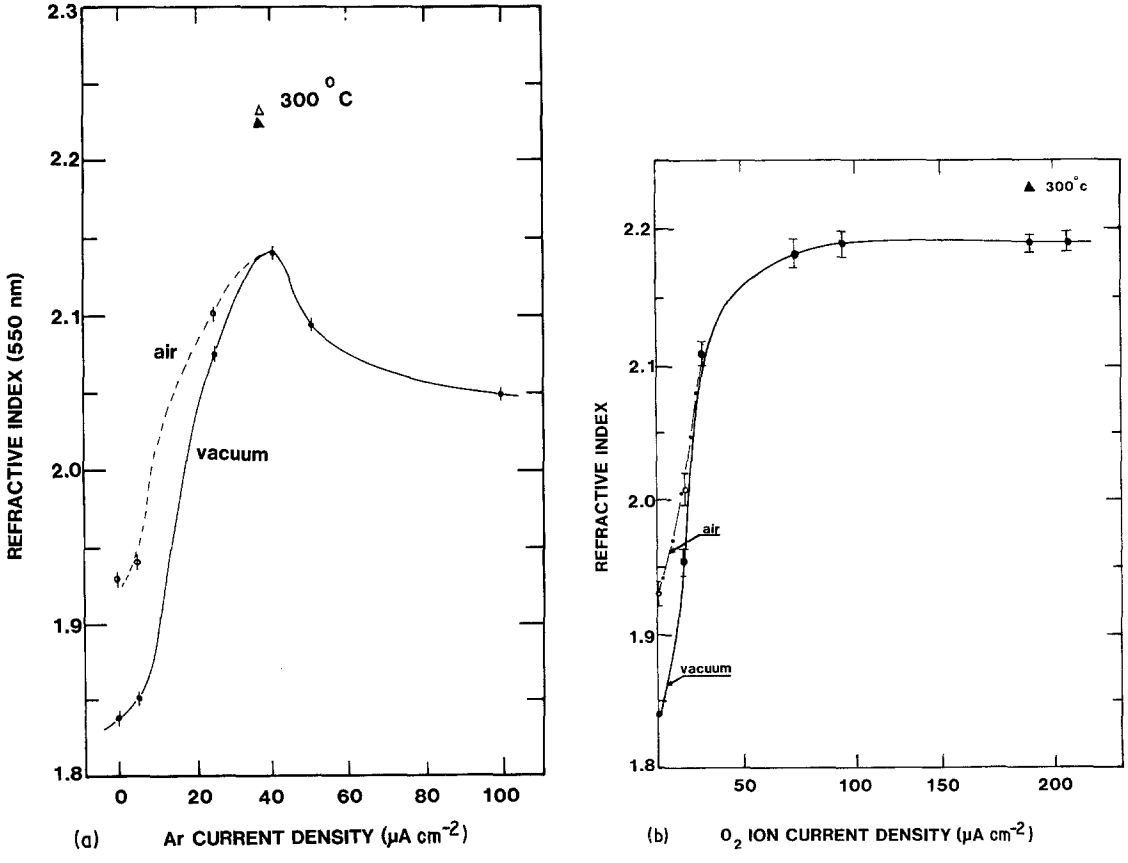

Figure 23 The refractive index of ZrO_2 at 550 nm measured in vacuum and air as a function of ion current density; (a) argon ions, (b), oxygen ions [43].

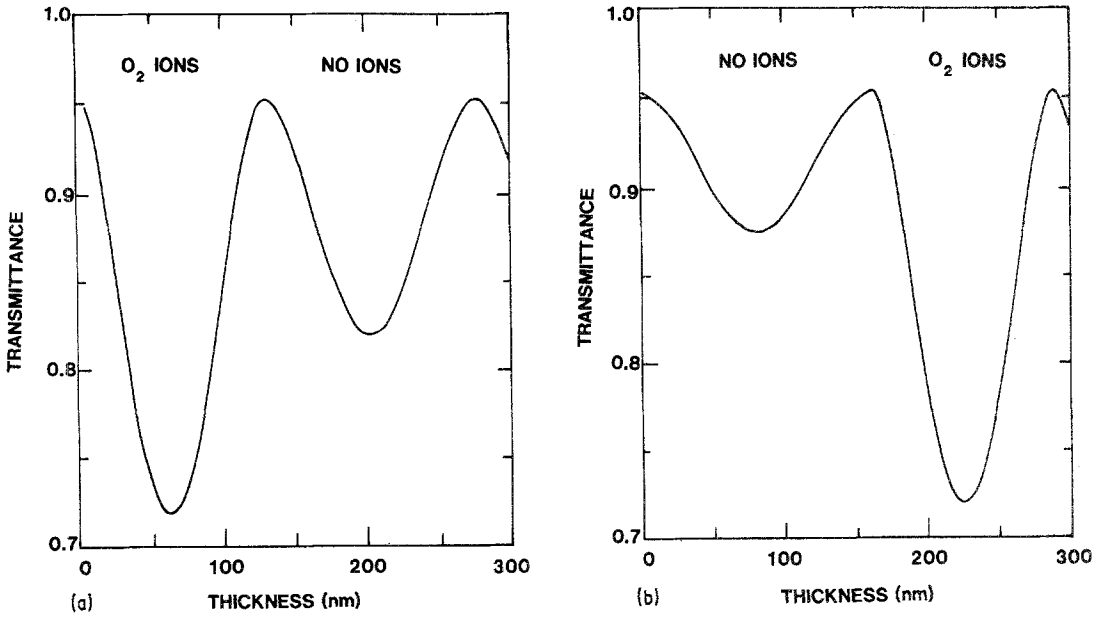

Figure 24 Transmittance of ZrO_2 films at 550 nm as a function of thickness for depositions; (a) with ion beam on (n = 2.18) – ion beam off (n = 1.9), and (b) beam off (n = 1.75) – beam on (n = 2.18) [43].

decay from the maximum value of 2.4 is observed at high current densities which is thought to be a result of trapping of unbound oxygen in the film and/or preferential sputtering effects. The mass difference between cerium and oxygen is sufficiently great that some preferential sputtering is to be anticipated. The packing density of films deposited without ions is quite low at about 0.5 but as with ZrO_2, the packing density can be improved with the ions to unity. Table VIII summarizes the refractive indices of CeO_2 prepared by ion-based methods.

6.6. Tantalum pentoxide

The final dielectric oxide discussed in our materials review is tantalum oxide. Tantalum oxide is readily prepared by sputtering either an oxide target or an elemental tantalum target in an oxygen atmosphere. For oxide targets a 90 : 10 partial pressure mixture of argon and oxygen is usually selected for both diode and ion-beam sputtering [111, 112]. The percentage of oxygen is usually increased to at least 25% for tantalum targets to reduce optical absorptance in the films. Ta_2O_5 has also been deposited using electron-beam evaporation of Ta_2O_5 although considerable outgassing of the source material occurs and oxygen backfilling must be employed to minimize absorption.

TABLE VII Refractive indices of ZrO_2 films produced by ion-based techniques

Wavelength λ (μm)	Refractive index n	Reference
0.25	2.47	86
0.40	2.2	86
0.55	2.15	86
	2.19	
0.80	2.15	86
1.00	2.15	86
1.06	2.15	86
	2.20	115
1.11	2.10	106

The optical properties are also sensitive to substrate temperature and deposition rate [113]. Ion-assisted deposition has been used to obtain high index material (2.1, 550 nm, [114]) but no detailed investigations have yet been reported, although preferential sputtering effects are known to be important in low energy bombardment of Ta_2O_5 [13]. Fig. 26 shows the data reported to date of films prepared by various techniques.

6.7. Carbon films

In the early 1970s it was found that ion-beam deposition could be used to deposit thin films of insulating carbon on room temperature substrates. The material was found to have remarkable properties and has since been the subject of intense investigation for many applications. Aisenberg and Chabot [47] described this material as diamond-like carbon (DLC)

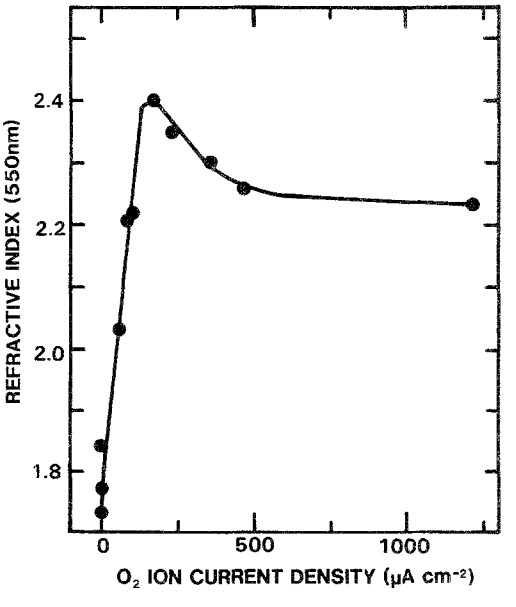

Figure 25 The refractive index of CeO_2 films at 550 nm as a function of oxygen ion current density [110].

TABLE VIII Refractive indices of CeO_2 films produced by ion-based techniques

Wavelength λ (μm)	Refractive index n	Reference
0.55	2.4	110
0.56	2.5	115
0.58	2.49	115
0.76	2.45	115
1.06	2.45	115
5.00	2.25	148
10.00	2.10	148

and listed the following characteristics (1) high transparency, (2) index of refraction greater than 2.0, (3) highly insulating, (4) harder than glass, (5) resistant to chemical attack, (6) diamond-like crystal structure and (7) dielectric constant between 8 and 14. The method adopted was deposition of carbon ions produced in a coaxial ion source by argon sputtering of a solid carbon electrode. The positive ions produced were then accelerated by a negative potential of -40 V applied to the substrate. The original experiments of Aisenberg and Chabot were later repeated by Spencer *et al.* [125] using a similar ion source to produce a beam of positively charged carbon ions of energy 50 to 100 eV. These measurements also showed the presence of polycrystalline cubic diamond, high resistivities $> 10^{12}\,\Omega$m and a refractive index of about 2.0.

It has now been demonstrated that DLC films can be deposited by r.f. plasma decomposition from a hydrocarbon gas such as butane, low energy carbon ion beam deposition, ion plating and dual-ion-beam-sputtering. The films are sometimes referred to as i-carbon (i-C) to indicate that ions are used in the deposition process. This term was introduced by Weismantel *et al.* [126] who studied the preparation and properties of i-C in some detail. However, some workers prefer the descriptive name amorphous hydrogenated carbon (a-C : H), particularly for films produced by plasma decomposition from hydrocarbons. Films prepared by this technique have variable optical constants depending upon the hydrogen

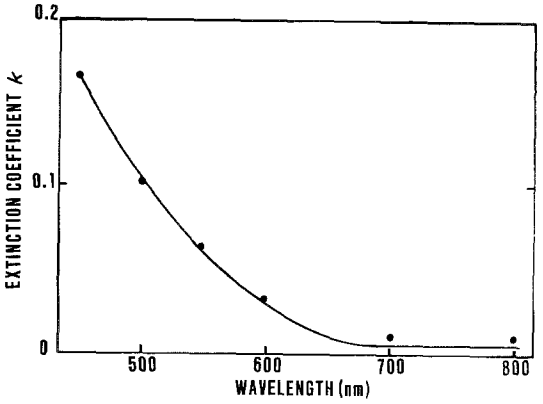

Figure 27 Extinction coefficient for ion-beam-deposited carbon films grown with 300 eV C^+ ions [128].

content and are frequently found not to contain diamond-like crystallities. In contrast, films deposited by direct ion-beam deposition often show evidence of diamond-like structure.

DLC films are attractive since they are hard, have a high index and a low optical absorption, at least in the infrared region. Bubenzer *et al.* [127] have tested DLC as a laser material and found CO_2 single-pulse damage thresholds for CO_2 laser pulses on anti-reflection-coated germanium up to 2.8×10^6 MW m^{-2}. The films were chemically resistant, stable to 250° C and had a hardness of 1200 to 1650 kg mm^{-2}.

The optical properties of a-C : H can be tailored to render it suitable for anti-reflecting germanium. The optical absorption in the 8 to 12 μm range is 250 cm^{-1} compared to about 10 cm^{-1} for ZnS. The absorption in the visible region is relatively high and Fig. 27 shows the extinction coefficient of a film deposited by a mass separated 300 eV C^+ ion-beam [128]. An example of the transmittance and absorptance variation in the visible for ion-beam sputtered films is shown in Fig. 28 for a 174 nm thick film [129]. Fig. 29 shows the much higher transmittances observed for ion-beam deposited films (44 nm thick) over the wavelength range 4 to 20 μm compared to that of evaporated carbon. DLC films have also been prepared by r.f. decomposition of various hydrocarbon source gases [130].

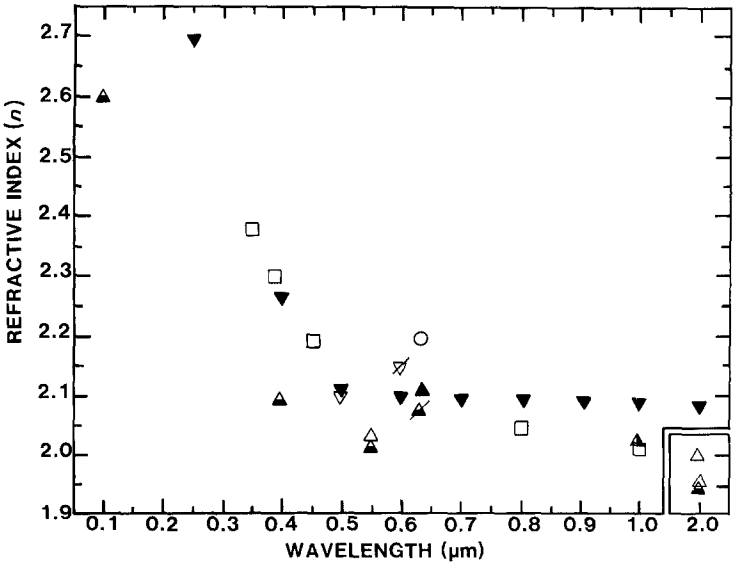

Figure 26 Summary of the dispersion of refractive index of Ta_2O_5 films produced by ion-based techniques. Various methods; Sputtering △ [95], ▼ [111], ▲ [112], ▲ [120], ⊿ [121], △ [122], ▽ [124]. Reactive evaporation □ [113]. IAD, ○ [114].

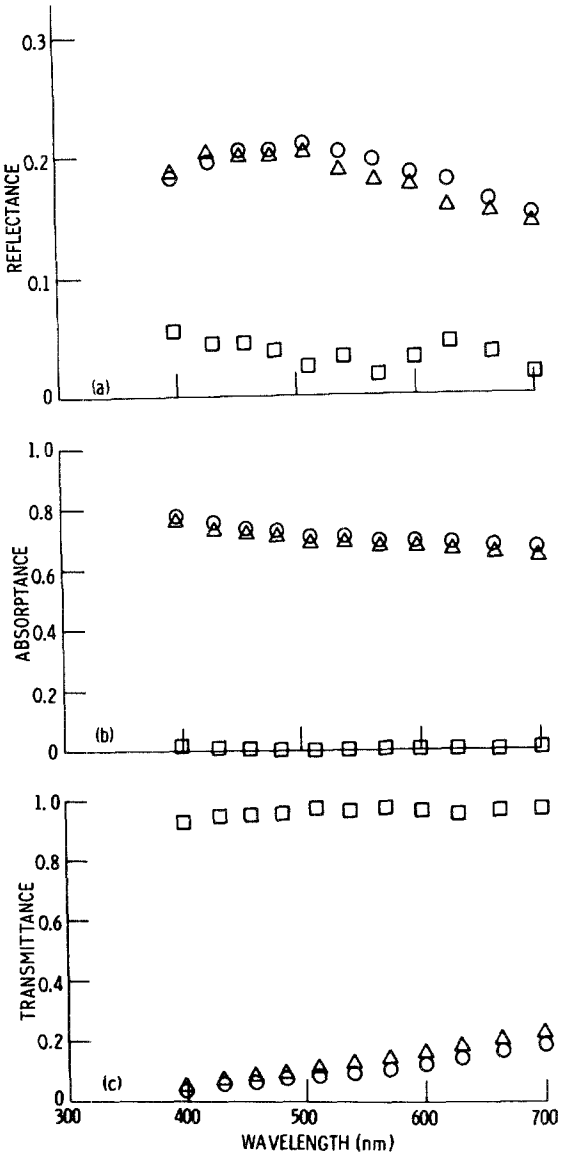

Figure 28 (a) Reflectance, (b) absorptance and (c) transmittance of thin diamond-like carbon films prepared by sputter deposition and ion-assisted-sputter-deposition techniques [129]. △, Sputter deposited only (166.8 nm thick). ○, Simultaneously sputter deposited and ion bombarded (173.8 nm thick). □, Uncoated fused silica (0.762 mm thick).

The optical properties of DLC films prepared by glow-discharge deposition and ion-beam sputtering have been accurately measured over the wavelength range 254 to 633 nm by Khan *et al.* [131]. Film thicknesses were approximately 120 to 150 nm and the optical properties measured by ellipsometry. The n and k values for films deposited by both techniques were the same. It was found that annealing the films in hydrogen at a temperature of 500° C had only a slight effect on the optical properties.

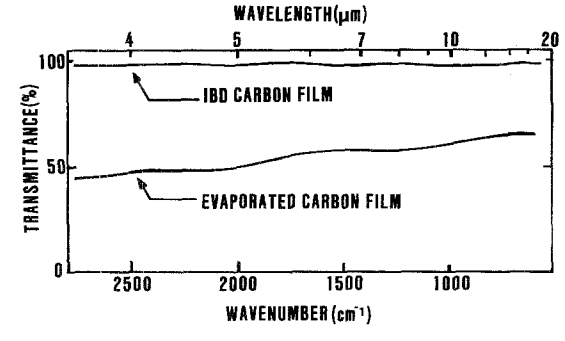

Figure 29 Transmission spectra of an ion-beam-deposited carbon film (44 nm) deposited using 300 eV C^+ and evaporated carbon [128].

The main problem with DLC as an optical material is the high optical absorption in the visible. The adhesion is poor on certain substrates such as copper, and the films are often highly stressed. Films deposited by either d.c. or r.f. glow-discharge decomposition of hydrocarbon gas can contain large amounts of incorporated hydrogen which result in a very high intrinsic compressive stress of the order of 10^{13} Nm^{-2} [132]. The material is already finding applications in the military field, in particular as a scratch resistant IR-transmitting coating on missile domes and is being produced by the Hughes Corporation (California, USA) on an industrial scale by the dual-ion-beam sputtering technique [133]. As the technology develops DLC will find wider applications as a protective and high index antireflective coating with good resistance to chemically aggressive gases.

6.8. Other Materials

Only a few investigations have been made on other optical thin films produced by ion-based techniques. Silicon nitride has been synthesized by ion-beam sputtering [44], and by reactive sputtering [134]. Amorphous hydrogenated silicon is presently under intensive investigation for applications in solar devices and ion-beam techniques have been used successfully in its preparation [135].

Tin oxides and indium–tin oxide are frequently prepared by sputtering and a comprehensive review of these and other conducting transparent coatings has been made by Vossen [136] and Dawar and Joshi [137]. Epitaxial zinc selenide and zinc sulphide films have been prepared by Jones *et al.* [138, 139]. The films were produced by r.f. sputtering with reproducible refractive indices close to the bulk values.

Attempts to deposit dense stable magnesium fluoride films on unheated substrates by sputtering have largely been unsuccessful. Coleman [115] showed that sputtering of MgF_2 targets produced absorbing films due to dissociation. Films with acceptable optical properties were produced by sputtering in Freon 14 but had extremely poor adhesion. Kennemore and Gibson [140] have reported on the deposition of hard, adherent MgF_2 films on ambient temperature substrates by low-energy argon-ion assistance. However, the films were found to contain substantial quantities of oxygen.

7. Applications

7.1. Multilayer coatings

Reactive sputtering has been shown to be a promising method for the production of multilayer coatings [134] and a number of dielectric optical multilayer filters have been made. In addition, electrically conducting transparent indium–tin oxide, silicon nitride and amorphous hydrogenated silicon have also been deposited. Multilayer optical edge filters of exceptional stability in humid atmospheres were fabricated with Si_3N_4 and SiO_2 for use in the visible region. The

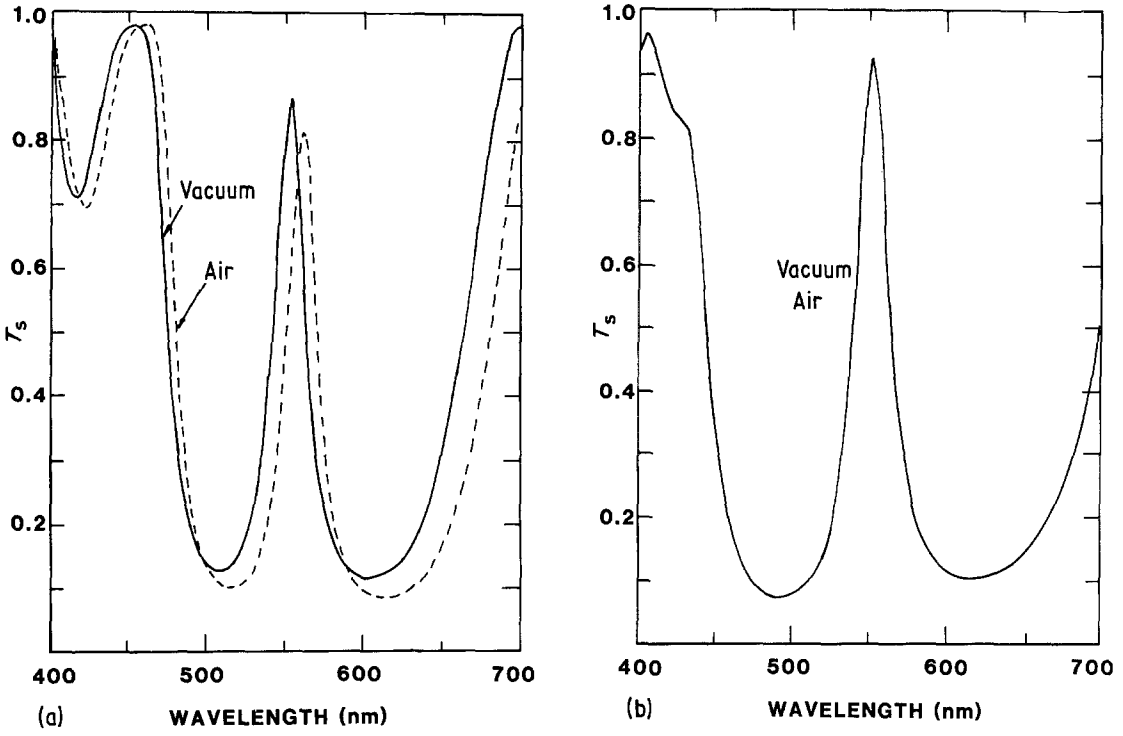

Figure 30 (a) Spectral transmittance of a fifteen-layer filter produced by evaporation of ZrO_2 and SiO_2 layers. Broken line is data in air. H-ZrO_2 and L-SiO_2, no ion beam. $(HL)^4$ $(LH)^4$. (b) Spectral transmittance of an eleven-layer filter produced by ion-assisted-deposition. No vacuum-to-air effects were observed [70]. H-ZrO_2 and L-SiO_2, with ion beam. $(HL)^3$ $(LH)^3$.

50% transmittance point shifted by less than 2 nm after 15 months at 85° C in a relative humidity of 85%.

Fig. 30 shows the effect of IAD on the stability of a ZrO_2(H), SiO_2(L) multilayer narrowband filter. The shift in the spectral transmittance of the evaporated filter on exposure to air is due to absorption of water vapour throughout the layers. When prepared by IAD the filter was stable to less than 0.5 nm. The stability is a consequence of film densification by ion-assistance which also produces layers with higher refractive indices. Hence the 11 layer IAD filter had the same bandwidth as a 15 layer evaporated filter.

7.2. Material mixing

Ion-based deposition techniques are well suited for mixing materials to obtain a range of optical properties. Sputter deposition is independent of the material melting points and under controlled conditions is suitable for depositing stoichiometric dielectric films. Motovilov and Rudina [118] have deposited mixtures of tantalum, niobium, zirconium, and titanium oxides with silicon dioxide by sputtering from two cathodes.

Material mixing can also be produced by reactive deposition. Silicon oxynitride SiO_xN_y can be synthesized by several techniques to vary the refractive index from 1.46 to 2.0. The most successful method used to date has been liquid phase chemical vapour deposition although promising results have been obtained by reactive sputtering, reactive evaporation, and ion-assisted deposition [40, 141, 142]. Heitmann found a refractive index of 1.6 at 633 nm for freshly deposited films with nitrogen ion-assisted deposition of SiO. However, the film index was reduced to 1.47 and the UV transmittance increased once the films were heated to 350° C for 9 h, indicating the instability and incomplete reaction of oxynitride formation for his deposition conditions. Infrared measurements were used to estimate a film composition of about 14% Si_3N_4 the remainder being SiO_2.

The ability of ion-based techniques to synthesize compounds will undoubtedly find greater application in dielectric optical films once the deposition conditions and operating parameters are established.

7.3. Optical waveguides

The use of ion-based techniques in dielectric film deposition has resulted in films with better optical properties than those prepared by simple evaporation. For the fabrication of integrated optical circuits, it is necessary to deposit thin-film waveguides with low optical loss and free from scattering effects. Optically transparent materials with a high refractive index in the range 2 to 3 are of interest in planar optical systems design. They are required in the fabrication of the waveguide layers on semiconducting materials with high refractive indices and materials with non-linear electro-optic and acousto-optic properties, and in the fabrication of planar optical elements (lenses, prisms, reflectors etc.).

A profile for ideal waveguide materials has been formulated by Pitt [143],

1. Good refractive index selectivity with a precision of one part in 10^4.
2. Accurate control of film thickness, since this determines the energy propagation velocity in the guide. A precision of a least one part in 10^3 per centimetre of guiding path is required.
3. Low absorption loss at the excitation wavelength.
4. Minimum scattering defects to achieve a total loss (absorption plus scattering) of less than 1 dB cm^{-1}.
5. A configurable geometry is required in order to define the device shape.

Waveguides are fabricated by various techniques such

as diffusion, sputtering, ion-implantation and chemical vapour deposition. However, waveguides produced by normal evaporation are unsuitable because of the variations in refractive index and scattering. Guided wave losses can be varied over the range 50 to 1 dB cm^{-1} by increasing the substrate temperature [144].

Waveguides produced by IAD show greater promise. Initial results by Binh *et al.* [90] show a loss of 1.54 dB cm^{-1} for Al_2O_3 prepared by oxygen-ion assisted deposition on room temperature substrates. Sputtering is frequently used to deposit Ta_2O_5 optical waveguides. Ingrey *et al.* [145] have deposited waveguides with losses < 1 dB cm^{-1} by d.c. diode sputtering of tantalum in oxygen–nitrogen mixtures. Ion-beam sputtering of tantalum with oxygen and argon results in absorbing films with a high-loss of 11 dB cm^{-1} [146], which was attributed to absorption rather than scattering. Other sputtered oxides have also been investigated for waveguide applications including niobium pentoxide with a waveguide loss of less than 2 dB cm^{-1} [147].

7.4. High power laser coatings

A major area of interest in inertial-confinement fusion and molecular laser isotope separation programmes is the development of damage-resistant optical coatings. Many materials have been investigated for laser damage resistance including most dielectric oxides [86, 95]. Titanium oxide films have been found to have a high threshold when in a glassy (no long-range order) rather than a polycrystalline state. The grain size is controllable if reactive sputter deposition is used. The highest threshold reported for titania is 8.7 ± 1.5 J cm^{-2} (1 nsec pulse, 1064 nm, over 2 mm beam diameter). Glassy Ta_2O_5 optical coatings were found to be less damage resistant than TiO_2 and failed at 3.0 ± 0.5 J cm^{-2} under the same conditions. Transparent indium–tin oxide coatings also have high damage thresholds of 5 to 6 J cm^{-2} when prepared by r.f. reactive sputtering.

Misiano *et al.* [148] have also used ion-beam and r.f. sputtering to prepare laser coatings. Damage thresholds were measured for Y_2O_3, CeO_2 and TiO_2 under various laser conditions and Y_2O_3 was found to have a threshold twice that of TiO_2 while CeO_2 was intermediate.

Ion-assisted deposition can also be used to improve damage resistance as demonstrated by Ebert [89] for multilayer coatings for use with ArF excimer lasers operating at 193 nm. A 34 layer broad band BeO–SiO_2 multilayer mirror achieved a reflectance of 99% and a damage threshold of 7.2 ± 0.8 J cm^{-2} (15 nsec pulse), an improvement of 4 and 10 times over that of Al_2O_3–SiO_2 and al_2O_3–MgF_2 multilayers respectively.

The precise mechanisms of film damage under laser irradiation have yet to be established and many factors such as film structure, uniformity, absorptance and surface defects are all influential to some degree. The use of sputtering and ion-assisted techniques has demonstrated that these methods can raise damage thresholds and will undoubtedly receive increasing attention in laser materials research.

7.5. Protective layers

Coatings are frequently used to protect thin-films and substrates which are susceptible to chemical or abrasive degradation. A good example is the metal layers on astronomical mirrors. Cole *et al.* [149] have shown that ion-beam sputtered Y_2O_3 films are much less permeable to water than evaporated coatings for protective layers on diamond turned aluminium mirrors.

Sainty *et al.* [150], have reported on the deposition of protective oxide layers on aluminium and silver mirrors by IAD. Thin films of Al_2O_3, SiO_2 and ZrO_2 were deposited on aluminium coated substrates under varying conditions. The substrates were immersed in a solution of NaOH and the etch rate monitored by observing the optical transmission. Similar experiments were performed on silver coated substrates this time by overcoating with either SiO_2 or ZrO_2 and etching in HNO_3. In both sets of experiments it was found that the greatest protection against film etching was achieved with an overcoat layer of 120 nm ZrO_2 deposited with ion-assistance. The improvement against etching was almost two orders of magnitude over that of an unprotected film. The improvement is explained as a consequence of the reduction of film porosity by ion-assisted deposition preventing penetration of film etchant to the metal layer. Such applications of IAD should find great application in extending the lifetime of large astronomical mirrors which may be subjected to chemical attack.

8. Summary

The kinetic energy of the depositing atoms in a growing film strongly influences the properties of the resulting thin film structure. The optical properties are particularly sensitive to the film microstructure and control over microstructure development is highly desirable. It has now become possible to control film microstructure by the use of ions either indirectly by sputter deposition techniques or directly by ion-assisted film growth enabling highly stable films to be grown with bulklike optical properties. Directed ion beams are likely to see greater use as the technology develops for depositing new types of coatings such as DLC and compound films as well as further improving the properties of dielectric oxide multilayers. A greater understanding of the growth processes involved should also result from computer simulations of atom by atom film growth coupled with ion-surface interaction phenomena.

Acknowledgements

The author wishes to thank R. P. Netterfield and K. H. Müller for permission to include recent unpublished data and M. Tychsen for assistance in preparing the figures.

References

1. E. RITTER, *Appl. Opt.* **20** (1981) 21.
2. M. KAMINSKY, "Atomic and Ionic Impact on Metal Surfaces" (Springer-Verlag, Berlin, 1965).
3. G. CARTER and J. S. COLLIGON, "Ion Bombardment of Solids" (Elsevier Publishing Company Inc., New York, 1968).

4. J. C. PIVIN, *J. Mater. Sci.* **18** (1983) 1267.
5. R. BEHRISCH, "Sputtering by Particle Bombardment, Topics in Applied Physics", Vol. 52, edited by R. Behrisch (Spring-Verlag, Berlin, 1983).
6. D. E. HARRISON, P. W. KELLY, B. J. GARRISON and N. WINOGRAD, *Surf. Sci.* **76** (1978) 311.
7. P. SIGMUND, *Phys. Rev.* **184** (1969) 383.
8. *Idem, Rev. Roum. Phys.* **17** (1972) 832.
9. *Idem, ibid.* **17** (1972) 969.
10. M. P. SEAH, *Thin Solid Films* **81** (1981) 279.
11. J. BODHANSKY, J. ROTH and H. L. BAG, *J. Appl. Phys.* **5** (1980) 2861.
12. H. H. ANDERSEN and H. L. BAY, in "Sputtering by Ion Bombardment" edited by R. Behrisch (Springer-Verlag, Berlin, 1980) p. 145.
13. E. TAGLAUER, *Appl. Surf. Sci.* **13** (1982) 80.
14. R. HOLM and S. STORP, *Appl. Phys.* **12** (1977) 101.
15. J. W. COBURN, *Thin Solid Films* **64** (1979) 371.
16. R. KELLY and N. LAM, *Rad. Effects* **19** (1973) 1.
17. H. M. NAGUIB and R. KELLY, *ibid.* **25** (1975) 1.
18. J. A. BRINKMAN, *J. Appl. Phys.* **25** (1954) 961.
19. H. L. BAY, B. SCHWEER, P. BOGEN and E. HINTZ, *J. Nucl. Mater.* **111** (1982) 732.
20. K. WITTACK, in "Inelastic Ion-Surface Collisions" edited by N. H. Tolk, J. C. Tully, W. Heiland and C. W. White (Academic Press, New York, 1981) p. 1.
21. K. MEYER, I. K. SCHULLER and C. M. FALCO, *J. Appl. Phys.* **52** (1981) 5803.
22. T. MOTOHIRO and Y. TAGA, *Surf. Sci. Lett.* **134** (1983) L494.
23. *Idem, Thin Solid Films* **112** (1984) 161.
24. A. W. KLEINSASSER and R. A. BUHRMAN, *Appl. Phys. Lett.* **37** (1980) 841.
25. H. D. HAGSTRUM, *Phys. Rev.* **96** (1954) 336.
26. J. A. THORNTON, *Thin Solid Films* **107** (1983) 3.
27. R. J. MacDONALD and P. J. MARTIN, *Surf. Sci* **111** (1981) L739.
28. W. ECKSTEIN and H. VERBEEK, "Data on Light Ion Reflection" IPP Report 9/32, (Max Planck Institut, Garching, FRG, 1979).
29. K. MORITA and T. TABATA, *J. Appl. Phys.* **55** (1984) 776.
30. G. CARTER, *J. Vac. Sci. Technol.* **7** (1969) 31.
31. U. LITTMARK and J. F. ZIEGLER, "Handbook of Range, Distribution for Energetic Ions in All Elements" (Pergamon, New York, 1980).
32. J. P. BIERSACK and L. G. HAGGMARK, *Nucl. Instrum. Methods* **174** (1980) 257.
33. G. CARTER and D. G. ARMOUR, *Thin Solid Films* **80** (1981) 13.
34. J. E. GREENE, *CRC Crit. Rev. Solid State & Mater. Sci.* **11** (1984) 47.
35. K. I. CHOPRA, *Appl. Phys. Lett.* **7** (1965) 140.
36. R. F. BUNSHAH and A. C. RAGHURAM, *J. Vac. Sci. Technol.* **9** (1972) 1385.
37. R. F. BUNSHAH, *Thin Solid Films* **107** (1983) 21.
38. D. M. MATTOX, *J. Vac. Sci. Technol.* **2** (1964) 283.
39. *Idem, ibid.* **10** (1973) 47.
40. W. HEITMANN, *Appl. Opt.* **10** (1971) 2414.
41. H. R. KAUFMAN, *J. Vac. Sci. Technol.* **15** (1978) 272.
42. H. R. KAUFMAN, J. J. CUOMO and H. M. E. HARPER, *ibid.* **21** (1982) 725.
43. P. J. MARTIN, R. P. NETTERFIELD and W. G. SAINTY, *J. Appl. Phys.* **55** (1984) 235.
44. C. WEISSMANTEL, *Thin Solid Films* **92** (1982) 55.
45. J. A. THORNTON and A. S. PENFOLD in "Thin Film Processes" edited by J. L. Vossen and W. Kern (Academic Press, New York, 1978) P. 75.
46. B. S. DANILIN and V. K. SIRCHIN, *Prib-Tekh. Eksp.* **4** (1978) 7.
47. S. AISENBERG and R. CHABOT, *J. Appl. Phys.* **42** (1971) 2953.
48. K. H. GUENTHER, *Appl. Opt.* **23** (1984) 3731.
49. S. NAKAHARA, *Thin Solid Films* **64** (1974) 149.
50. B. A. MOVCHAN and A. V. DEMCHISHIN, *Phys. Met. Metallogr.* **28** (1969) 83.
51. J. A. THORNTON, *J. Vac. Sci. Technol* **11** (1974) 666.
52. *Idem, ibid.* **12** (1975) 830.
53. R. MESSIER, "Are Thin Films Fractals?" in Proceedings of the 3rd International Conference on Solid Films and Surfaces, Sydney, August 1984, *Appl. Surf. Sci.* in press.
54. R. A. OUTLAW and J. H. HEINBOCKEL, *Thin Solid Films* **108** (1983) 79.
55. J. SALIK, NASA Technical Memorandum 83559 (1984).
56. D. HENDERSEN, M. H. BRADSKY and P. CHAUDHARI, *Appl. Phys. Lett.* **25** (1974) 641.
57. S. KIM, D. HENDERSON and P. CHAUDHARI, *Thin Solid Films* **47** (1977) 155.
58. A. G. DIRKS and H. J. LEAMY, *ibid.* **47** (1977) 219.
59. H. J. LEAMY, G. H. GILMER and A. G. DIRKS, "Current Topics in Materials Science", Vol. 6, edited by E. Kaldis (North-Holland, Amsterdam 1980) p. 309.
60. K. H. MÜLLER, *Thin Solid Films* (in press).
61. S. OGURA, N. SUGAWARA and R. HIRAGA, *ibid.* **30** (1975) 3.
62. S. OGURA, PhD thesis, Newcastle upon Tyne Polytechnic, 1975.
63. D. M. MATTOX and G. J. KOMNIAK, *J. Vac. Sci. Technol* **9** (1972) 528.
64. R. F. BUNSHAH and R. S. JUNTZ, *ibid.* **9** (1972) 1404.
65. D. DOBREV and M. MARINOV, *C. R. Acad. Bulg. Sci.* **26** (1973) 231.
66. M. MARINOV and D. DOBREV, *Thin Solid Films* **42** (1977) 265.
67. M. MARINOV, *ibid.* **46** (1977) 267.
68. D. DOBREV, *ibid.* **92** (1982) 41.
69. V. O. BABAEV, Ju. V. BYKOV and M. B. GUSEVA, *ibid.* **38** (1976) 1.
70. P. J. MARTIN, H. A. MACLEOD, R. P. NETTERFIELD, C. G. PACEY and W. G. SAINTY, *Appl. Opt.* **22** (1983) 178.
71. W. D. MÜNZ and D. HOFMANN, *Metall.* **37** (1983) 279.
72. J. DUDONIS and L. PRANEVICIOUS, *Thin Solid Films* **36** (1976) 117.
73. L. PRANEVICIOUS, *ibid.* **63** (1979) 77.
74. G. I. GRIGOROV, I. N. MARTEV and K. K. TZATSOV, *C. R. Acad. Bulg. Sci.* **32** (1979) 1069.
75. W. HEITMANN, *Appl. Opt.* **10** (1971) 2419.
76. K. I. CHOPRA, "Thin Film Phenomena" (McGraw-Hill, New York, 1969) P. 134.
77. P. J. MARTIN, R. P. NETTERFIELD and W. G. SAINTY, *Appl. Opt.* **23** (1984) 2668.
78. E. H. HIRSCH and K. VARGA, *Thin Solid Films* **52** (1978) 445.
79. J. J. CUOMO, J. M. E. HARPER, C. R. GUARNIER, D. S. YEE, L. J. ATTANSIO, J. ANGILLELO, C. T. WU and R. H. HAMMOND, *J. Vac. Sci. Technol.* **20** (1982) 349.
80. T. TAKAGI, *Thin Solid Films* **92** (1982) 1.
81. T. HAYASHI, H. OKAMOTO and Y. HOMMA, *Jpn J. Appl. Phys.* **19** (1980) 1005.
82. E. RITTER, *Vak-Tech.* **21** (1972) 42.
83. G. REALE, *Bulg. Akad. Nauk.* **31** (1978) 281.
84. T. H. ALLEN, in Proceedings of the Society of Photo-Optical Instrumentation Engineers, Los Angeles, January 1982, edited by R. I. Seddon (SPIE, Washington, 1982) p. 93.
85. *Idem,* in Proceedings of the International Ion Engineering Congress, Kyoto, September 1983, edited by T. Takagi (Ionics Co., Tokyo, 1983) p. 1305.
86. W. T. PAWLEWICZ, D. D. HAYS and P. M. MARTIN, *Thin Solid Films* **73** (1980) 169.
87. R. S. NOWICKI, *J. Vac. Sci. Technol.* **14** (1977) 127.
88. C. DESHPANDEY and L. HOLLAND, *Thin Solid Films* **96** (1982) 265.
89. J. EBERT, in Proceedings of the Society of Photo-Optical Instrumentation Engineers, Los Angeles, January 1982, edited by R. I. Seddon (SPIE, Washington, 1982) p. 29.
90. L. N. BINH, R. P. NETTERFIELD and P. J. MARTIN, "Low Loss Optical Waveguiding in Ion-Beam-Assisted-Deposited Thin Films", in Proceedings of the 3rd International Conference on Solid Films and Surfaces, Sydney

(1984), *Appl. Surf. Sci.* in press.
91. R. ROY and W. B. WHITE, *J. Cryst. Growth* **13** (1972) 78.
92. K. G. GERAGHTY and L. F. DONAGHEY, *Thin Solid Films* **40** (1977) 375.
93. H. K. PULKER, G. PAESOLD and E. RITTER, *Appl. Opt.* **15** (1976) 2986.
94. W. GROSSKLAUS and R. F. BUNSHAH, *J. Vac. Sci. Technol.* **12** (1975) 593.
95. W. T. PAWLEWICZ and R. BUSCH, *Thin Solid Films* **63** (1979) 251.
96. S. SCHILLER, G. BEISTER, W. SIEBER, G. SCHIRMER and E. HACKER, *ibid.* **83** (1981) 239.
97. K. SUZUKI and R. P. HOWSON, in Proceedings of the International Ion Engineering Congress, Kyoto, 1983, edited by T. Takagi (Ionics Co., Tokyo, 1983) p. 889.
98. K. TAKIGUCHI, S. OGAWA and Y. TAKAHASHI, in Proceedings of the International Ion Engineering Congress, Kyoto, 1983, edited by T. Takagi (Ionics Co., Tokyo, 1983) p. 1337.
99. H. KUSTER and J. EBERT, *Thin Solid Films* **70** (1980) 43.
100. J. R. McNEIL, A. C. BARRON, S. R. WILSON and W. C. HERRMAN, *Appl. Opt.* **23** (1984) 552.
101. M. N. CHEREPONOVA and N. F. TITOVA, *Sov. J. Opt. Technol.* **46** (1979) 694.
102. G. A. MURANOVA, E. I. FADEEVA and A. F. PERVEEV, *ibid.* **44** (1977) 682.
103. R. HIRAGA, N. SUGAWARA, S. OGURA and S. AMANO, *Jpn. J. Appl. Phys. Suppl.* **2** (1) (1974) 689.
104. A. F. PERVEEV, A. V. MIKHAILOV, G. A. MURANOVA and V. V. LL'IN, *Sov. J. Opt. Technol.* **42** (1975) 6.
105. A. F. PERVEEV, L. A. CHEREZOVA and A. V. MIKHAILOV, *ibid.* **44** (1977) 122.
106. J. E. GREENE, R. E. KLINGER, L. B. WELSH and F. R. SZOFRAN, *J. Vac. Sci. Technol.* **14** (1977) 177.
107. W. T. PAWLEWICZ and D. D. HAYS, *Thin Solid Films* **94** (1982) 31.
108. V. V. KLECHKOVSKAYA, V. I. KHITROVA, S. I. SAGITOV and S. A. SEMILTOV, *Sov. Phys. Crystallogr.* **25** (1980) 636.
109. C. MISIANO and E. SIMONETTI, *Vacuum* **27** (1977) 403.
110. R. P. NETTERFIELD, private communication (1984).
111. E. E. KHAWAJA and S. G. TOMLIN, *Thin Solid Films* **30** (1975) 361.
112. J. R. SITES, Air Force Weapons Laboratory Report TR-83-13 (Kirtland, New Mexico, 1983).
113. W. C. HERRMANN, *J. Vac. Sci. Technol.* **18** (1981) 1303.
114. L. BINH, private communication (1984).
115. W. J. COLEMAN, *Appl. Opt.* **13** (1974) 946.
116. L. L. MATSKEVICH and V. V. BAZHINOV, *Sov. J. Opt. Technol.* **44** (1977) 98.
117. L. L. MATSKEVICH and V. A. CHERNYAYSHII, *ibid.* **46** (1979) 179.
118. O. A. MOTOVILOV and O. G. RUDINA, *ibid.* **41** (1974) 329.
119. M. VARASI, C. MISIANO and L. LASAPONARA, in Proceedings of the International Ion Engineering Congress, Kyoto, September 1983, edited by T. Takagi (Ionics Co., Tokyo, 1983) p. 1041.
120. R. H. DEITCH, E. J. WEST, T. G. GIALLORENZI and J. F. WELLER, *Appl. Opt.* **13** (1976) 712.
121. H. TERUI and M. KOBAYUSHI, *Appl. Phys. Lett.* **32** (1978) 666.
122. F. RUBIO, J. M. ALBELLA, J. DENIS and J. M. MARTINEZ-DUART, *J. Vac. Sci. Technol.* **21** (1982) 1043.
123. S. SCHILLER, U. HEISIG, K. STEINFELDER and J. STRUMPFEL, *Thin Solid Films* **63** (1979) 369.
124. S. SCHILLER, G. BEISTER, S. SCHNEIDER and W. SIEBER, *ibid.* **72** (1980) 475.
125. E. G. SPENCER, P. H. SCHMIDT, D. C. JOY and F. J. SANSALONE, *Appl. Phys. Lett.* **29** (1976) 118.
126. C. WEISSMANTEL, K. BEWILOGUA, D. DIETRICH, H. J. ERLER, H. J. HINNEBERG, S. KLOSE, W. NOWICK and G. REISSE, *Thin Solid Films* **72** (1980) 19.
127. A. BUBENZER, B. DISCHLER, G. BRANDT and R. KOIDL, *Opt. Eng.* **23** (1984) 153.
128. T. MIYAZAWA, S. MISAWA, S. YOSHIDA and S. GONDA. *J. Appl. Phys.* **55** (1984) 188.
129. A. BANKS and S. K. RUTLEDGE, *J. Vac. Sci. Technol.* **21** (1982) 807.
130. P. G. TURNER, R. P. HOWSON and C. A. BISHOP, in Proceedings of the 2nd International Conference on Low Energy Ion Beams, Bath, (Institute of Physics, Bristol, 1980) p. 229.
131. A. A. KHAN, D. MATHINE, J. A. WOOLLAM and Y. CHUNG, *Phys. Rev. B.* **28** (1983) 7229.
132. D. NIR, *Thin Solid Films* **112** (1984) 41.
133. R. S. CLARK, *Photonics Spectra* **18** (1984) 97.
134. W. T. PAWLEWICZ, P. M. MARTIN, D. D. HAYS and I. B. MANN, in Proceedings of the Society of Photo-Optical Instrumentation Engineers, Los Angeles, January 1982, edited by R. I. Seddon (SPIE, Washington, 1982) p. 105.
135. P. J. MARTIN, R. P. NETTERFIELD, W. G. SAINTY and D. R. McKENZIE, *Thin Solid Films* **100** (1983) 143.
136. J. L. VOSSEN, in "Physics of Thin Films", edited by G. Hass, M. H. Francome and R. W. Hoffman, Vol. 9 (Academic Press, New York, 1977) p. 1.
137. A. L. DAWAR and J. C. JOSHI, *J. Mater. Sci.* **19** (1984) 1.
138. P. L. JONES, D. MOORE and D. R. COTTON, *J. Crystal Growth* **59** (1982) 183.
139. P. L. JONES, D. R. COTTON and D. MOORE, *Thin Solid Films* **88** (1982) 163.
140. C. M. KENNEMORE and U. J. GIBSON "Ion-Beam Processing for Coatings onto Ambient Temperature Substrates" in Technical Digest of Optical Interference Coatings, Monterey (Optical Society of America, 1984).
141. R. I. FRANK and W. L. MOBERG, *J. Electrochem. Soc.* **117** (1970) 524.
142. T. S. ERIKSSON and C. G. GRANQVIST, *Appl. Opt.* **22** (1983) 3204.
143. C. W. PITT, *Thin Solid Films* **86** (1981) 137.
144. T. T. H. KERSTEN, H. F. MAHLEIN and W. RAUSCHER, *ibid.* **28** (1975) 369.
145. S. J. INGREY, W. D. WESTWOOD, F. C. LIVERMORE, R. J. BOYNTON and B. K. MACLAURIN, *ibid.* **35** (1976) 1.
146. W. D. WESTWOOD and S. J. INGREY, *J. Vac. Sci. Technol.* **13** (1976) 104.
147. R. L. AAGARD, *Appl. Phys. Lett.* **27** (1975) 605.
148. C. MISIANO, M. VARASI, C. MANCINI, P. SARTORI and L. LASAPONARA, in Proceedings of the 9th International Vacuum Congress and 5th International Conference on Solid Surfaces, Madrid, September 1983, edited by J. L. de Segovia (Asociacion Española del Vacio y sus Aplicaciones, Madrid, 1983) p. 132.
149. B. E. COLE, T. J. MORAVEC, R. G. AHONEN and L. B. EHLERT, *J. Vac. Sci. Technol.* **A2** (1984) 372.
150. W. G. SAINTY, R. P. NETTERFIELD and P. J. MARTIN, *Appl. Opt.* **23** (1984) 1116.

Received 19 February
and accepted 13 March 1985